PHYSICAL-AND-MATHEMATICAL MODEL OF PENETRATORS INTO MULTILAYER MEDIA IN THE PRESENCE OF LARGE PULSED CURRENTS AND SUBSTANTIATE WITH DEMIONSTRATION EXPERIMENTS

Final Scientific and Technical Report, Item 0003

By
A.F. Piskunkov, Dr., Principal Investigator,
N.P. Shishaev, Dr., V.A. Obukhov, Dr.

September 1998

United States Army
EUROPEAN RESEARCH OFFICE OF THE U.S. ARMY
London, England
CONTRACT NUMBER 68171-98-M-5655
R&D no: 8524-AN-01
R&D PLATONIK LTD
Moscow, Russia

REPORT DOCUMENTATION PAGE			Form Approved OMB No. 0704-0188
Public reporting burden for this collection of information is estimated to average 1 hour per response, including the time for reviewing instructions, searching existing data sources gathering and maintaining the data needed, and completing and reviewing the collection of information. Send comments regarding this burden estimate or any other aspect of this collection of information, including suggestions for reduction this burden, to Washington Headquarters Service, Directorate for information Operations and Reports, 1215 Jefferson Davis Highway, Suite 1204 Arlington, VA 22202-4302, and to the office of Management and Budget, Paperwork Reduction Project (0704-0188), Washington, DC 20503.			
1.AGENCY USE ONLY (Leave blank)	4. Report Date: 31 July 99	3. Report type and dates covered 1 Jan 99 – 31 Jul 99	
4. TITLE AND SUBTITLE: Physical-and-mathematical model of penetrators into multilayer media in the presence of large pulsed currents and substantiated with demonstration experiments.			FUNDING NUMBERS C. 68171-98-M-5655
6. AUTHORS: A. F. Piskunkov, N. P. Shishaev, V. A. Obukhov			
7. PERFORMING ORGANIZATION NAME(S) AND ADDRESS(ES) R&D PLATONIK Ltd.125871 Moscow, Volokolamskoe shosse, 4. Russia			8. PERFORMING ORGANIZATION REPORT NUMBER: 002E-98
9. SPONSORING/MONITORING AGENCY NAME(S): EUROPEAN RESEARCH OFFICE OF THE U.S. ARMY. USARDSG-UK. Edison House. 223 Old Marylebone Road. LONDON NW1 5TH.			10.SPONSORING/MONITORING AGENCY REPORT NUMBER
11. SUPPLEMENTARY NOTES Interim Report on Item 0002 of the Contract.			
12a. DISTRIBUTION/AVAILABILITY STATEMENT			12b. DISTRIBUTION CODE
13. ABSTRACT. Physical-and-mathematical model of interaction processes in cumulative jet (CJ) influenced by pulsed electric current as physical basis of electrodynamics armor (EDA) has been studied. Magnetohydrodynamics model of CJ with current has been formulated. The role of the current integral and the rate of the discharge current growth as the main factors influencing the penetration deepness decrease have been shown. The critical magnitudes of both parameters as dependencies on jet charge caliber has been calculated. The parametric analysis of coordination of the discharge circuit parameters and dimensions of EDA on the base of numerical modeling has been done. The theoretical estimations provide the design of EDA experimental assemblies for EDA efficiency demonstration and the theoretical model checking. Two groups of experiments namely: with laboratory jet charges and with standard 2-100-mm jet charges has been conducted. The experimental and theoretical results are discussed. Technical problems of EDA realization and experimental modeling are discussed. It has been demonstrated that two and more times' decrease of the penetrating deepness can be provided at battery capacity of units of *mF*, discharge voltage 5-10 *kV* for jet charge caliber 20 – 100 mm.			
14. SUBJECT ITEMS Electrodynamics armor, cumulative jet penetration, physical-mathematical model, current integral, current grow rate, EDA laboratory investigations, full-scale tests.			15. NUMBER OF PAGES.47 16. PRICE CODE
17. SECURITY CLASSIFICATION OF REPORT	18. SECURITY CLASSIFICATION OF THIS PAGE	19. SECURITY CLASSIFICATION OF ABSTRACTS	20. LIMITATION OF ABSTRACTS SAR

INITIATOR LIST

Piskunkov A.F, PHD, Chief of Department, Principal Investigator

Shishaev N.P., PHD, Senior Scientist

Obukhov V.A., PHD, Senior Scientist, R&D PLATONIK

Svotina V.V., Scientist

ABSTRACT

Physical-and-mathematical model of interaction processes in cumulative jet (CJ) influenced by pulsed electric current as physical basis of electrodynamics armor (EDA) has been studied. Magnetohydrodynamics model of CJ with current has been formulated. The role of the current integral and the rate of the discharge current growth as the main factors influencing the penetration deepness decrease have been shown. The critical magnitudes the both parameters as dependencies on a jet charge caliber has been calculated. The parametric analysis of coordination of the discharge circuit parameters and dimensions of EDA on the base of numerical modeling has been done. The theoretical estimations provide the design of EDA experimental assemblies for EDA efficiency demonstration and the theoretical model checking. Two groups of experiments namely: with laboratory jet charges and with standard 80-mm jet charges has been conducted. The experimental and theoretical results are discussed. Technical problems of EDA realization and experimental modeling are discussed. It has been demonstrated that two and more times' decrease of the penetrating deepness can be provided at battery capacity of units of *mF*, discharge voltage 5-10 *kV* for jet charge caliber 20 – 80 mm.

CONTENT

KEYWORDS

Electrodynamics armor, cumulative jet penetration, pulsed current, physical-mathematical model, current integral, current grow rate, EDA laboratory investigations, full-scale tests.

ABBREVIATION AND DESIGNATION

ES	Explosive substance
CB	Capacitor battery
CJ	Cumulative jet
EDA	Electrodynamics armor
ЭДС	Electromotive force
W_C	CB energy
W_r	Energy allocated in active resistance
V_C	CB voltage
J	Electric current
J_0	Discharge current
J_m	Discharge current maximum value
t_m	Time of the $J_0 = J_m$ achievement
$\bar{J}_0$	Discharge current average value
q_0	CB charge
J_0^{cr}	Discharge current critical value
J_{cr}	Critical maximum value of the current in the cavity
t_{cr}	Time of J_{cr} current formation
B	Magnetic field induction
C	CB capacity
d	Interelectrode spacing value
dW	Volume element
M_0	Active part of CJ mass
D	caliber
E	Electrical field
$\bar{j}_0$	Average density of the current in CJ
j	Density of induced current
γ	Circuit parameter
$\tilde{I}$	Current integral for conductor explosive vaporization
I	Current integral in electrodynamics model
I_{ion}	Atom ionization potential
l	Jet part length between electrode and contact surface
L	CJ penetration deepness to the target
L_0	CJ-without-current-penetration deepness
L_m	CJ-with-current-penetration Deepness
L_i	Circuit inductance
L_{i0}	Circuit inductance per unit of length
n	Atom concentration in plasma
n_0	Atom concentration in metal
P	Pressure
P_{cr}	Critical pressure
P_G	Hydrodynamics pressure
P_M	Magnetic pressure
r	CJ cross-section radius
$\bar{r}$	CJ resistance average value
r_0	CJ initial radius
r_1	Plasma channel radius
r_C	Cavity radius
r_s, θ	Contact Surface Spherical Coordinates
ψ	Material strength tensile
R	Circuit active resistance
$\tilde{R}$	CJ external radius
R_0	Resistance value per unit of length
R_C	CJ resistance per unit of length
R_p	Plasma channel resistance
S	CJ cross-section
t	Penetration time
T_{BH}	Full time of CJ penetration
T_{cr}	Critical temperature
T_F	Fermi temperature
T_I	Current pulse duration
T_V	Atom vaporization temperature
U	CJ penetration rate with current
U_0	CJ penetration rate without current
ΔU	Penetration rate valuation
$V(V_r, V_z)$	layer velocity, CJ velocity
V_0	Initial CJ velocity
V_{cr}	Rod critical rate
V_p	Plasma rate
Y	Material dynamic hardness
Z	Penetration deepness current value
α	Angle between CJ and normal to electrode
δ	Damping decrement
δ_{CK}	Skin-layer thickness
μ	Magnetic permeability
ρ	electrode material density
ρ_C	Jet material density
σ	CJ material conductivity
σ_0	Plasma conductivity
ν	CJ material viscosity
$\gamma = \frac{V_p}{\bar{U}}$	Plasma velocity to penetration rate ratio

INTRODUCTION

As it has been shown theoretically in [1, 2] cumulative jet (CJ) penetrability can be reduced by passing a pulsed current through CJ. The numerical estimation showed that this principal idea might be used for the realization of simple in design and technology electrodynamics armor (EDA) against jet charges (JC). The technology of demonstration experiments also could be easy realized. On the other hand the development of a reliable EDA using so limited means as the discharge of a capacitor battery (CB) through CJ does necessary to provide a number of modeling (methodical) experiments. This contract with limited financing did not give possibilities to provide "full-scale" research on all scientific and technological aspects of EDA. The main task of the present study is to develop a physical model of processes in EDA and to demonstrate the CJ penetrating deepness decrease under high pulsed current influence.

The presented report adds up the results of about one year activity of R&D PLATONIK scientific group.

In the report the parametric analysis of experimental results on cumulative jet (CJ) effected by a pulsed current is carried out.

The parametric analysis of theoretical and experimental results puts the following problems:

1. To show that the offered discharge physical-and-mathematical model takes into account basic physical processes in CJ under effect on a pulsed current. It allows to predict with an acceptable error relation of CJ penetration deepness in EDA from main recorded parameters - capacity and voltage of the condenser battery (CB), feeder line properties connecting CB and EDA in view of the CJ actual parameters (lengths and radius, maximum velocity, material). The analysis should takes into account the EDA structural diagram (quantity of electrodes, distance between them) and protected wall material performance.
2. To select among the current pulse parameters (steepness and duration, maximum and average discharge current values) the main ones determining the EDA efficiency.
3. To determine influence some parameters not arrested in everyone experiment, for example, jet resistance and resistance of "jet - electrode" contact on EDA efficiency, to show necessity to take into account them at statistical processing of the experiment results, to formulate requirements to decreasing their influence on EDA efficiency.

The physical-and-mathematical model of electrodynamics armor (EDA) that allows systematizing the experimental results and opens a capability to forecast the process parameters carries out such analysis.

The present report consists of 3 chapters and 4 appendices.

In chapter 1 the design formulas for CJ with current penetration deepness determination in different models described in Appendices 1 ... 3 are presented. The determination scheme of average current through CJ at given discharge circuit performance is shown.

In chapter 2 the laboratory experimental researches on CJ penetration into electrodynamics bumper system are described. The penetration deepness is compared with calculating value depending on circuit parameter $\gamma = \frac{R}{2}\sqrt{\frac{C}{L_i}}$, CB capacity and energy.

In chapter 3 the scheme and results of EDA full-scale tests by usage of nominal cumulative means are presented. The CJ of *90 mm* caliber penetration computational deepness as a function of the CB capacity and energy for different circuit resistance are presented. Appendices 1 ... 4 represent the computational models for CJ with current penetration deepness estimation.

In the report there are conclusions by major experimental and computational research results.

This report is final and is made according to item 0003 of Contract No. 68171-98-M-5655

1 ELECTRODYNAMICS ARMOR PARAMETER.S COORDINATION PROBLEM

EDA parameter coordination problem poses as a problem of its parametric optimization for the purpose of EDA maximum efficiency. EDA efficiency is estimated by CJ penetration decreasing factor $\frac{L_0}{L_m} \geq 1$ (L_0 – penetration deepness without current, L_m – penetration deepness with current). Values L_0, L_m are determined from the cavity axis dimension in a target (monolith bumper) in which the electrodes connected with CB.

The EDA parameters can be the following:

- adjusting (capacity C, voltage V_c);
- defining by the feeder line scheme selection and electrode system (discharge circuit inductance);
- depending on current closing conditions in interelectrode spacing and not inspected in experiment (active discharge circuit resistance R, including resistance of a discharge "electrode – jet" gap).

As a result the solution of the EDA parameter coordination problem the at which the influence of the last uncontrolled factor would be minimum condition should be determined. The problem is decided by usage of the physical-and-mathematical model permitting to predict the EDA efficiency function from its parameters.

The EDA parameter coordination problem breaks up on some individual problems.

1.1 CONSEQUENCES FROM PHYSICAL EDA MODEL

The basis of a physical model of the electrodynamics interaction on CJ is the description of the generation mechanism of the induced by CJ motion currents $jr \sim \sigma V_c B$ ($B = \frac{\mu J_0}{2\pi r_0}$ – magnetic field induction created by discharge current J_0; V_0, r_0 – CJ velocity and radius, σ – CJ material conductivity) in discharge current magnetic field. In case of pulse current interaction the Lorentz force braking a material is affixed on a thin CJ skin-layer (t – current pulse duration, μ – magnetic constant, $\delta_{CK} \sim \sqrt{\frac{t}{\pi\sigma\mu}}$). The thermal energy generated per unit of volume in time unit is $\sim \sigma B^2 V_0^2$.

Jet kinetic energy converted to thermal one for the time δt is calculated as:

$$\sigma B^2 V_0^2 \delta t \sim \frac{\rho V_0^2}{2}$$

(ρ – CJ material density).

Taking into account $\sigma \sim 10^6$ $(\Omega \times m)^{-1}$, $\rho = 8 \times 10^3$ kg/m^3 it is possible to receive $J \sim 100$ kÀ, registered in the electrodynamics interaction on CJ experiments [1, 2] at $\delta t \sim 10^{-5}$ sec.

The specific heat of copper vaporization at temperature is higher than melting point [3] that is equals to 4.7×10^6 *J/kg*. The specific jet kinetic energy is $\frac{V_0^2}{2} \sim 3 \times 10^7$ *J/kg*. It is possible to expect an explosive evaporation of CJ mass concluded in a skin-layer if the specific thermal energy generated in a skin-layer exceeds ~ *20 %* of jet specific kinetic energy. In this case the plasma sheath can be organized near to a jet. Thus, the plasma located in high-pressure area will be possible to have imperfect plasma properties.

The latter is proved by estimation of the pressure and temperature critical values determining plasma transition in the condition with metallic conduction. For copper this estimation can be conducted under the formula:

$$P_{cr} = 0.4 I_{ion}^4; \; T_{cr} = 0.04 I_{ion},$$

where:

$I_{ion} = 7.5$ *eV*.

Whence $P_{cr} \sim 10^8$ *N/m*^{2}, $T_{cr} \sim 0.3$ *eV*.

Definite thus pressure is about magnetic field pressure (at the current of about ~*100 kA*):

$$P_M = \frac{\mu J^2}{8\pi^2 r_0^2} \sim 10^8 \; N/m^2$$

and is less then jet hydrodynamics pressure:

$$P_G = \frac{\rho V_0^2}{2} \sim 10^{11} \; N/m^2.$$

The plasma channel which conductivity can be close to a conductivity of a metal can short current. It could be if a current in metallic conductor flows inside thick skin-layer which thickness is $\delta_{CK} << r_0$ So, according to non-classical skin-layer model for the plasma channel [1] it is possible to consider that the magnetic field and the current occupies the whole plasma volume.

As both plasma critical temperature $T_{cr} \sim 0.3$ *eV* ~ 4×10^3 *K* and temperature relevant to latent heat of atom vaporization ($T_V \sim 2$ *eV* ~ 3×10^4 *K*) are less than Fermi temperature ($T_F = 4.3 \times 10^{-11} n^{\frac{2}{3}} \sim 10^5$ K at $n \sim 10^{23}$ *cm*$^{-3}$) the plasma conductivity can be determined as in [3]:

$$\sigma \sim \sigma_0 \frac{n}{n_0},$$

where:

$\sigma_0 = 10^6$ *(Ω×m)*$^{-1}$;

n, n_0 atom concentration in plasma and metal, correspondingly.

As earlier [1, 2] the model in which $n \sim \frac{1}{r^2}$ and $\sigma = \sigma_0 \frac{r_0^2}{r^2}$ is used.

The linear resistance R_p of the plasma channel at $r_0 < r < r_1$ corresponds to the jet cross-section:

$$\frac{1}{R_p} = \int_{r_0}^{r_1} \sigma(r) 2\pi r dr = \sigma_0 2\pi r_0^2 \ln\frac{r_1}{r_0}.$$

The jet linear resistance R_C depends on the jet radius and the skin-layer thickness δ_{CK} as follows:

$$\frac{1}{R_C} = \sigma_C 2\pi r_0 \delta_{CK}\ ;\ \delta_{CK} \sim \sqrt{\frac{\tau}{\pi\sigma\mu}}.$$

Taking into account $\sigma_0 \sim 10^6\ (\Omega\times m)^{-1}$, $\sigma_C \approx 4.7\times 10^6\ (\Omega\times m)^{-1}$ (copper conductivity at melt point), $\delta_{CK}\ (at\ \tau \sim 5\ \mu sec) \sim 0.5\,mm$, $r_0 \sim 1\,mm$, $\ln\frac{r_1}{r_0} \approx 2$ it is possible to receive

$$R_p \sim R_C \sim 0.35\times 10^{-2}\ \Omega$$

Thus, the estimations give the identical value for the resistance of both the plasma channel and the jet. The interelectrode spacing resistance might be determined experimentally and being presented in Fig.1 is close to the obtained estimation.

In a plasma flowing from the cavity with the velocity about V_p an EMF can be generated as a result of the interaction between discharge current J_0 and a magnetic field in the cavity [1].

$$EMF = \int_{r_1}^{r_C} BV_p dr \cong V_p \frac{\mu J_0}{2\pi} \ln\frac{r_C}{r_1} = V_p J_0 Li_0,$$

where:

Li_0 linear inductance of a current circuit in the cavity.

When the plasma flow velocity achieves a value of rate V_p a loop with a current that is irrelevant to the discharge current can appear in the cavity. This model assumes that the energy of the induced current in the cavity is taken mainly from the CJ kinetic energy but not from CB storage energy.

The implementation of the following scheme of CJ penetration process is possible under the electric current passing. At CJ velocity *5 ... 10 km/s* in a result of CJ partly skin-layer evaporation in the cavity a plasma can appear. In the magnetic field of the discharge current in the plasma the current of density $j_r \sim \sigma V_p B$ is induced. The interaction of the induced current with the magnetic field the Lorentz forces braking the flow arises. The pressure generating in the plasma is transmitted to CJ through the contact surface of the CJ head in the cavity. This process results decrease of the penetration velocity.

The mechanism of jet kinetic energy losses is possible at the radial target deformation caused by the CJ impact. As a result of radial velocity V_r the induced current of density $j_Z \sim \sigma V_r B$ appears. Both discharge and induced currents has to be similar direction. In this case the braking force operats against the magnetic pressure determined by current J_0 flowing in CJ or in the adjacent plasma channel. The magnetic

pressure at $J_0 \sim 100\ kA$ is equal to $P_M = \frac{\mu J^2}{8\pi^2 r_0^2} \sim 10^8\ N/m^2$. It is less than the hydrodynamics pressure component that equals to $P_G = \frac{\rho V_0^2}{2} \sim 10^{11}\ N/m^2$. However, the magnetic pressure force is determined as a product of the pressure on CJ lateral surface area, meanwhile the hydrodynamics pressure force is determined by CJ cross-section. Therefore at axial current through CJ the essential losses of the hydrodynamics pressure are possible. It offers to consider two mechanisms of electrodynamics action on CJ. The first one actuates plasma deceleration by the magnetic field. In so doing, pressure $p_p(r)$ in the plasma appears. Then CJ penetration rate U in the target (contact surface movement velocity) can be estimated from Bernoulli's equation:

$$P = \frac{\rho U^2}{2} + \psi + P_p = \frac{\rho_C (V_0 - U)^2}{2}, P_p = \frac{\int_0^{\frac{\pi}{2}} p_p(r)\cos\theta dS}{\pi r_0^2}, \ dS = 2\pi r_s^2 \sin\theta d\theta \qquad (1)$$

where:

ρ, ρ_C target and CJ material densities;

ψ target metal strength tensile;

V_0 CJ initial velocity;

dS element of the contact surface (written in spherical coordinate system);

r_s, θ spherical coordinates.

From Bernoulli's equation (1) the pressure P_p effects on CJ similar as the target material resistance defined by its strength tensile ψ. It leads to CJ penetration velocity U decreases (see Appendix 4). On the other hand the additional pressure onto the contact surface has to cause the cavity diameter increase as it is watched in experiments.

The second mechanism is caused by the hydrodynamics pressure action on the contact surface at the radial deformation in the magnetic field. For non-steady-state flow Bernoulli's equation is used for qualitative estimation of CJ velocity influence on the penetration rate. If to neglect the target material elastic resistance and to consider $\rho \sim \rho_C$ it is possible to receive:

$$\frac{\rho U^2(t)}{2} \sim \frac{\rho_C [V(t) - U(t)]^2}{2},$$

whence:

$$U(t) \cong \frac{1}{2} V(t).$$

For this mechanism CJ penetration velocity decrease is explained by CJ electrodynamics braking (jet velocity decrease).

1.2 INDUCED CURRENTS IN CUMULATIVE JET

In [1, 2] it has been shown, that the EDA efficiency depends on currents induced in the cavity. The model assumes the formation of current loops in the cavity irrelevant with the discharge current circuit. Such currents can not proceed the critical value defined by the discharge current building up $\frac{\partial J_0}{\partial t}$:

$$J_{cr} \cong \tilde{\gamma} \frac{\partial J_0}{\partial t} t_{cr}, \tag{2}$$

where:

t_{cr} time of the current growth in the front of the discharge current pulse.

Fig. 1 represents the experimental functions of discharge current $J_0(t)$ and resistance $R(t)$ of t at the conditions: CB capacity $C \sim 6 \times 10^{-3} F$, CB voltages $V_c = 21 kV$, CC caliber $D = 100\ mm$. The interelectrode spacing was executed under the double-electrode scheme.

Fig. 1 represents also the computational current pulse $J \cong J_{cr}$. The factor of the penetration deepness decrease for the given pulse duration $\tilde{T}_I$ can be calculated from the formula A1.5 (Appendix 1):

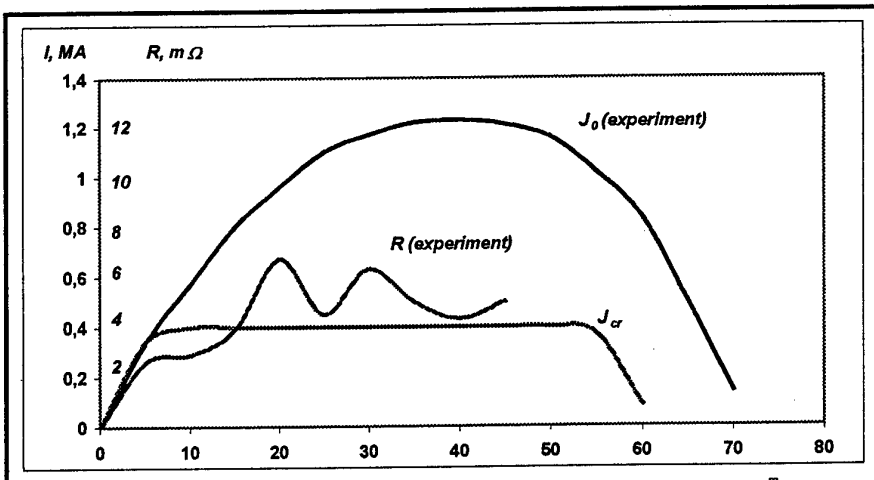

Fig. 1 Experimental and computational pulsed currents through CJ in the cavity (test 001)

$$\left(\frac{L_0}{L_m}\right)_{\tilde{T}_i} = 1 + \frac{I_I^2}{A_0},\ A_0 = \frac{6\pi M_0}{\sigma_0 \mu^2 V_0},\ J_{cr} = \tilde{\gamma} \frac{\partial J_0}{\partial t} t_{cr},\ \tilde{\gamma} \sim 2,\ I_I = J_{cr} \tilde{T}_i \tag{3}$$

where:

I_I current integral;

$M_0 = \rho \pi r_0^2 l_0$ mass of CJ active part with length of l_0;

$\sigma_0 = 10^6\ (\Omega \times m)^{-1}$ plasma conductivity;

For CJ of caliber D the following approximating relations were taken:

- radius $r_0 \sim \frac{1}{60} D$;

- total penetration deepness $L_0 \sim 4D$;
- jet length $l_0 \sim 8D$;
- total penetration time without current $T_{BH} \sim \frac{l_0}{V_0}$.

For mode presented in Fig. 1 $T_{BH} > \widetilde{T}_i$ ($T_{BH} \sim 100$ μsec, $\widetilde{T}_i \sim 60$ μsec) during period of time $\tau \sim T_{BH} - \widetilde{T}_i$ the current influence may be neglect. In this case the total penetration time may be estimated by the formula A1.6 (Appendix 1):

$$L_m = L_0 \left[\frac{1}{y + \frac{I^2}{A_0}} + 1 - \frac{1}{y} \right], \quad y = \frac{T_{BH}}{\widetilde{T}_i} \tag{4}$$

Fig. 2 gives the current in CJ of $D = 100$ mm for CB capacity 12.8 mF (test 002) and 19.2 mF (test 003), at voltages 5 kV.

Initial current growth rates in these modes are different:

$$\left.\frac{\partial J}{\partial t}\right|_{t=0} (002) \approx 4 \times 10^{10} \ A/sec$$

$$\left.\frac{\partial J}{\partial t}\right|_{t=0} (003) \approx 2 \times 10^{10} \ A/sec.$$

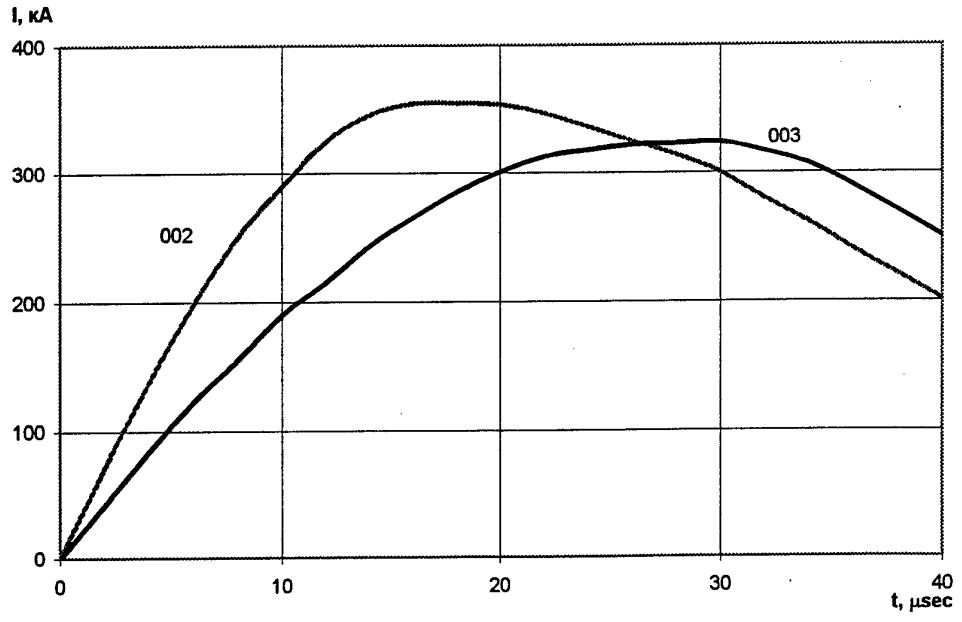

Fig. 2 Current-of-time dependencies in tests No. 002 and 003

As $\left.\frac{\partial J}{\partial t}\right|_{t=0} = \frac{V_C}{L_i}$, it is possible to receive:

$$\frac{L_i(003)}{L_i(002)} \sim 2.$$

For CJ of *100-mm* caliber $t_{cr} \sim 10\ \mu sec$ (Appendix 2) current $J_0 < J_{cr}(t_{cr})$ in tests *002* and *003* is observed at the greater part of the discharge pulses.

In this case the current estimation in cavity at average value of the CB discharge current $\bar{J}_0$ is possible to receive as (Appendix 2):

$$J_2(t) = \tilde{\gamma}\bar{J}_0 \frac{t_{cr}}{t}\left(1 - exp\left(-\frac{t}{t_{cr}}\right)\right). \tag{5}$$

Current integral equals to:

$$I_2 = \int_0^{T_i} J_1(t)dt \sim \tilde{\gamma}\bar{J}_0 t_{cr}\left(1 + ln\frac{T_i}{t_{cr}}\right). \tag{6}$$

It is possible to accept $I = min(I_1, I_2)$ as an estimated value of the current integral.

1.3 DETERMINATION OF DISCHARGE CIRCUIT PARAMETERS

In tests *001... 003* the maximum discharge current decreases at CB capacity increase from $C \sim 6$ *mF* (test *001)* to *12 mF* (test *002)*. In test *003* ($C \sim 18$ *mF*) maximum discharge current stayed on the level of test 002. Let us show that it is connected with the change of the active resistance of the discharge circuit. Let us estimate discharge circuit parameters not indicated in these tests using CB parameters (C, V_c) and current curve parameters (maximum current value J_m and time t_m of its achievement).

Fig. 3 from [3] represents the result of the estimation as dependencies on $\gamma = \frac{1}{2}R^2\sqrt{\frac{L_i}{C}}$ - parameter

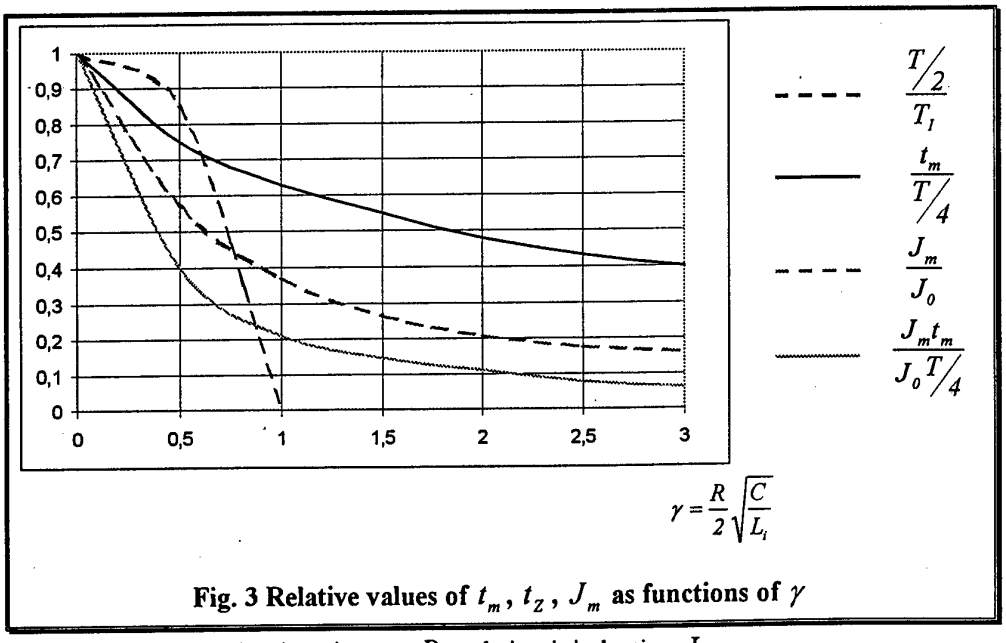

Fig. 3 Relative values of t_m, t_Z, J_m as functions of γ

giving available to calculate circuit resistance R and circuit induction L_i,

$T = 2\pi\sqrt{L_i C}$;

$J_0 = V_C\sqrt{\frac{C}{L_i}}$ maximum current value;

T_1 pulse duration.

Parameter γ determination allows to define circuit parameters using the data presented in Fig. 3 by calculating the following criteria: $y = \frac{2}{\pi}\frac{J_m t_m}{CV_c} = \frac{J_m t_m}{J_{00}\frac{T}{4}}$.

The operational sequences for γ, L_i, R determination are presented below.

Test 001:

$$y = 0.26,\ \gamma = 0.6,\ \frac{J_m}{J_{00}} = 0.45,\ J_{00} = V_C\sqrt{\frac{C}{L_i}} = 2.7\times 10^6\ A,\ L = 4\times 10^{-7}\ Henry,$$

$$R = 2\gamma\sqrt{\frac{L_i}{C}} = 10^{-2}\ \Omega.$$

The calculated value R is close to measured value given in Fig. 1.

Test *002:*

$$y = 0.07,\ \frac{J_m}{J_{00}} = 0.3,\ J_{00} = 1.2\ MA,\ L = 2.1\times 10^{-7}\ Henry,\ \gamma = 3,\ R = 24\ m\Omega$$

Test *003*:

$$y = 0.06,\ \frac{J_m}{J_{00}} = 0.3,\ J_{00} = 1.2\ MA,\ L = 4\times 10^{-7}\ Henry,\ \gamma = 3,\ R = 27\ m\Omega$$

Thus, the essential difference of discharge parameters in described tests is explained by parameter γ change that causes the change of the circuit resistance: $R(001) \sim 10\ m\Omega$, $R(002) \sim R(003) \sim 25\ m\Omega$

1.4 MODEL OF ELECTRODYNAMICS EFFECT ON CUMULATIVE JET

The theoretical model described in section 1.2 assumes the increase of target resistance to CJ penetrating in the case of plasma generation in the cavity. It is supposed that the plasma is generated at CJ skin-layer explosion evaporation accompanied by the CJ electrodynamics braking in the magnetic field of the discharge current. This model can be used for EDA efficiency estimation when the discharge current exceeds a critical value for a given CJ caliber. At smaller currents it is possible to guess that the plasma influence on EDA efficiency is negligible. For this case the effect of the penetration deepness decrease might be connected with CJ kinetic energy losses under CJ radial deformation in the magnetic field of the current passing through CJ. CJ deepness penetration can be estimated from the analytical solution of Navier-Stokes equations (Appendix 3, 4). At different assumptions two models are obtained.

MODEL 1:.

Penetration decrease factor is obtained as:

$$\frac{L_0}{L_m} = \left[\frac{L_0}{r_0}\right]^{\frac{1}{2}} \left[\frac{P_M}{P_G}\right]^{\frac{1}{4}}, \text{(for } L_o/L_m>1, \text{ see App.4)} \tag{7}$$

where:

L_0, L_m CJ penetration deepness with and without current;

$P_M = \frac{B^2}{2\mu} = \frac{\mu J_0^2}{8\pi^2 r_0^2}$ magnetic pressure;

$P_G = \frac{\rho V_0^2}{2}$ hydrodynamic pressure.

MODEL 2.

Penetration decrease factor is obtained as:

$$\frac{L_0}{L_m} = \left[\frac{L_0}{r_0}\right]^{\frac{2}{3}} \left[\frac{P_M}{P_G}\right]^{\frac{1}{3}}, \text{(for } L_o/L_m>1, \text{ see App.3)} \tag{8}$$

In these models the EDA efficiency is determined by two parameters: $\frac{L_0}{r_0}$ - relation between penetration deepness and CD radius when J_0=0, and $\frac{P_M}{P_G}$ - relation between magnetic and hydrodynamic pressure components.

In sections 3, 4 EDA efficiency estimations on different models and the comparison with experimental results will be conducted.

1.5 DETERMINATION OF DISCHARGE CURRENT AVERAGE VALUE

In offered models EDA efficiency was estimated taking the average (on pulse duration) current value. As it is shown in section 1.2 the mode with maximum efficiency at minimum (critical) capacity C_{cr} can be determined assuming $\gamma \sim \gamma_{cr}$

$$\gamma_{cr} = \frac{1}{2} R \sqrt{\frac{C_{cr}}{L_i}} = 1 \tag{9}$$

From (9) C_{cr} is defined by circuit parameters R, L_i.

The current at $\gamma = \gamma_{cr}$ is calculated by formula:

$$J_0^{cr} = \frac{V_C}{L_i} t \exp\left(-\frac{R}{2L_i} t\right). \tag{10}$$

The average current value in the critical mode is $(T_1 > T_{BH})$:

$$\bar{J}_0^{cr} = \frac{1}{T_{BH}} \int_0^{T_{BH}} J_{cr}(t) dt = \frac{V_C C_{cr}}{T_{BH}}. \tag{11}$$

The average current value in the mode with $\gamma \neq 1$ is determined by formula A2.7 (Appendix 2):

$$\bar{J} = \bar{J}_0^{cr} \frac{1+\gamma^2}{2\gamma^2} \frac{T_{BH}}{T_1}. \qquad (12)$$

From (12) at $\gamma \sim 0.8$ the average current value is $\bar{J} = \frac{2CV_C}{T_1}$. This value corresponds to the average discharge current value when the attenuation can be neglected:

$$\bar{J} = \frac{q_0}{T/4} = \frac{CV_C}{T/4} = \frac{2CV_C}{T_i}.$$

Equations (10)-(12) are received for *two-electrode-EDA*. In the case of *tree-electrode-EDA* the values calculated by these equations must be divided to 2.

1.6 EDA OF "ABSOLUTE EFFICIENCY"

For estimation it can be determined the parameters of ideal EDA (for example assuming factor $\frac{L_0}{L_m} \sim 100$).

According to (A3.13)

$$\frac{L_0}{L_m} = 2\left[\frac{l}{r_0}\right]^2 \frac{P_M}{P_G}, \qquad (13)$$

where: $l = d + L_m$, d - interelectrode spacing.

In case of $l = d_{cr}\left(L_m << d\right)$ one can receive

$$d_{cr} = r_0 \sqrt{\frac{L_0}{L_m}} \sqrt{\frac{1}{2}\frac{P_G}{P_M}} \qquad (14)$$

Value of d_{cr} determines the critical (minimum) spacing between electrodes for ideal EDA efficiency. At $J = 400\ \kappa A$, $r_0 \sim 1\,mm$, $\frac{P_G}{P_M} = 125$, interelectrode spacing $d_{cr} > 100\ mm$. This estimation is right at very high current growth rate when the penetration effect can be neglected.

2 LABORATORY EXPERIMENTAL INVESTIGATION OF CUMULATIVE JET PENETRATION

Principal diagram of the laboratory experiment is presented in Fig. 4.

In the first experimental series cumulative charge mock-ups (*1*) with copper conical funnels of *25-mm* caliber were used. Two-section CB of total capacity *600 μF* was connected with electrodes (*4, 6*) by a low-inductive high-voltage coaxial cable (*10*).

Basic plate 9 assembled from homogeneous aluminum alloy plates had total thickness of about *200 mm*. The thickness of fiberglass insulated plate (*5*) has the thickness Δ_1 in the range of *0...15 mm*, and the thickness of plate *7* Δ_2=*5... 10 mm*. CJ penetration deepness without current was up to $L_{0MAX} = 95$ *mm*.

Performance of three tests is presented in Table 1.

Current oscillograms registered using *RC*–integrator output connected with inductive sensor 11 are given in Fig. 5.

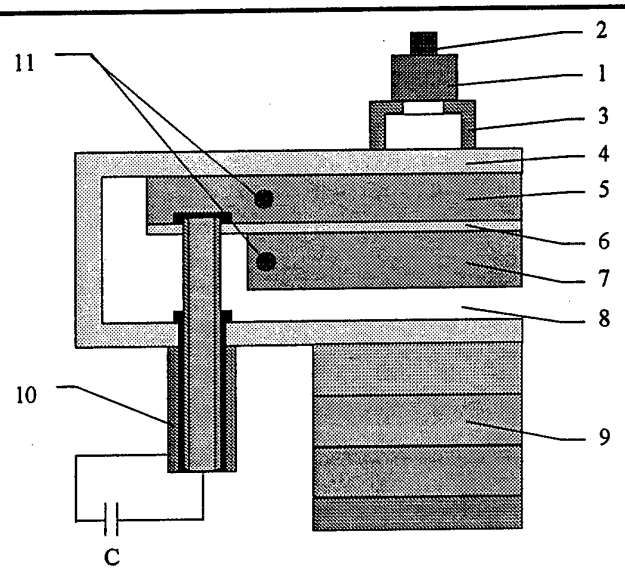

Fig. 4 Apparatus scheme for EDA laboratory investigation

1– Cumulative charge, 2 – Electric detonator, 3 – Fiberglass plate, 4, 6 – Copper electrodes (1 mm), 5 – Fiberglass (Δ_1, mm), 7 – Fiberglass (Δ_2, mm), 8 – Air Backlash (3 mm), 9 – Basic plate (target), 10 – High-voltage cable, 11 – Inductive sensor

Table 1

№	Test					Calculation				
	C, *mF*	V, *kV*	W, *kJ*	α, *deg*	L_0, *mm*	γ	R, *μΩ*	L, *μHenry*	L_m, *mm*	L_0/L_m
01	0.6	4.3	5.6	0	25	1	13	0.15	31	3
02	0.3		2.8		34	0.2	9		45	2.1
03				60	23	0.25	11		34	2.7

Experimental and calculated results are compared in table 1. One can see satisfactorily agreement of theoretically predicted data and experimental ones. The data were calculated at J_2 current (Fig. 5). For test *01* the current was assumed as $J = J_{max}\frac{t}{t_{max}}$; for tests *02* and *03* the average value of the discharge current was used. For test *03* the magnetic pressure was taken proportional to the current in square (calculated assuming model (Appendix 3)).

The formation of "ledge" at the cavity inlet for case of $\alpha=60^0$ share is shown in Fig. 6. This effect apparently is connected with the action of electromagnetic forces. However, influence of angle α on penetration deepness as it follows from calculation results, (table 1) is negligible.

The computational estimation of CJ radial expansion in the cavity for test 01 is given in Fig. 7a. Maximum relative CJ radius increase is $\left(\frac{R}{r_0}\right)_{max} \sim 3$. It corresponds to $T_1 \sim T_{BH}$ condition. CJ and cavity geometry are shown in Fig. 7 (not in scale). In Fig. 7b the calculated cavity radius at *two-times* current pulse decrease is given. One can see that at so different discharge parameters essential cavity form change can be observed.

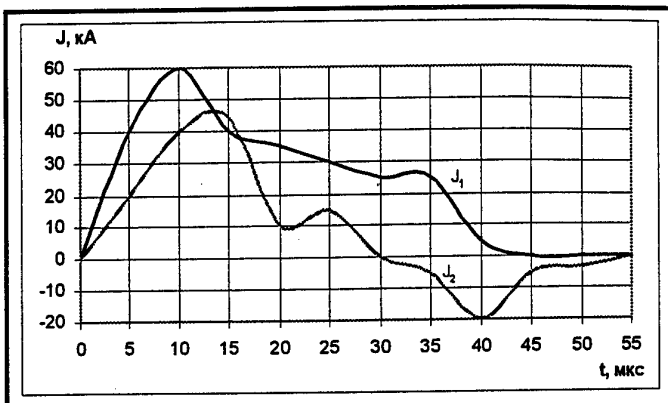

Test 01

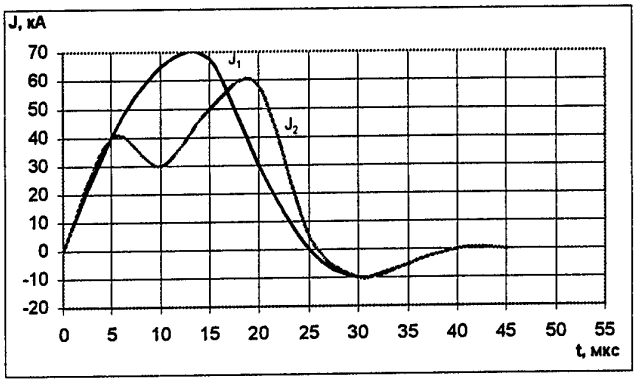

Test 02

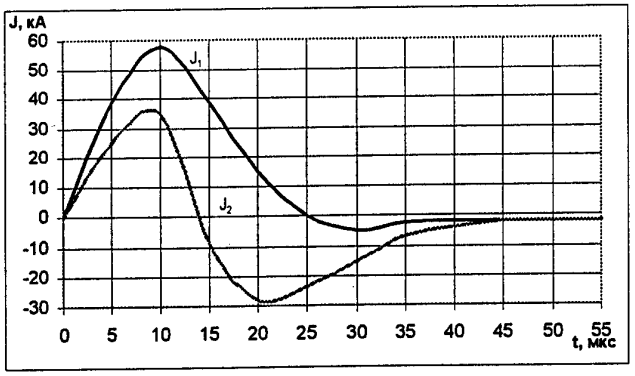

Test 03

J_1 – current in upper circuit (Fig. 3), J_2 – current in lower circuit

Fig. 5 Current function of time in tests No. 10, 18, 19

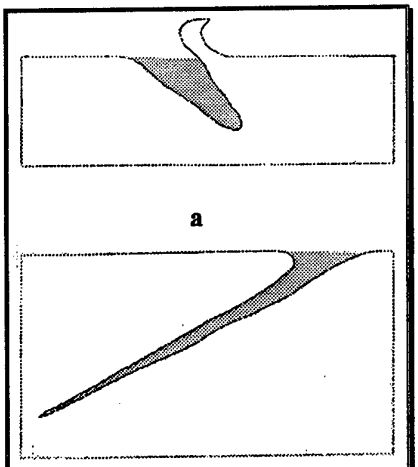

а

б

Fig. 6 Cavity forms for a 25-mm cumulative charge in aluminum target

а) Test with current (03); б) control test without current

Radial deformation for the case of CJ without current is seen only in place round the contact surface. For CJ with current the deformation is spread around the whole cavity.

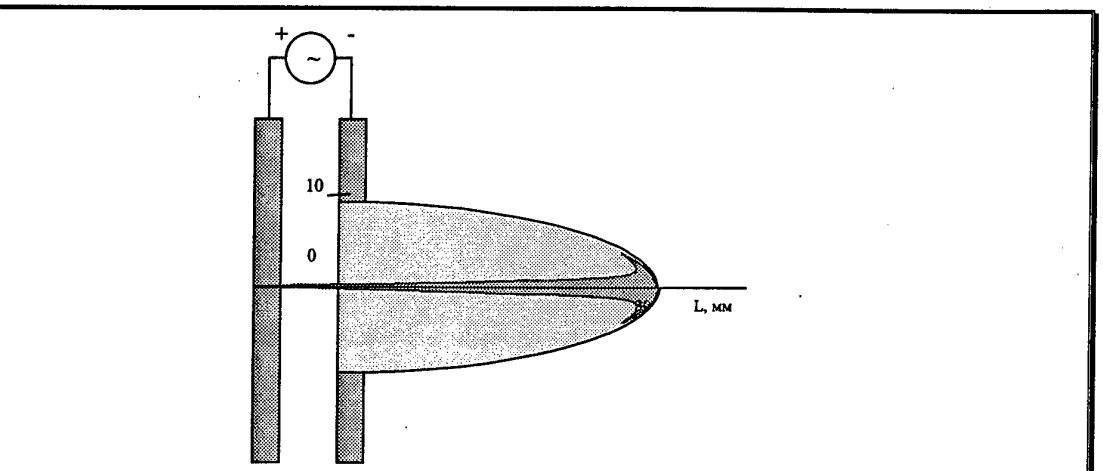

a) $t \le T_1$, $T_1 \sim T_{BH}$ case

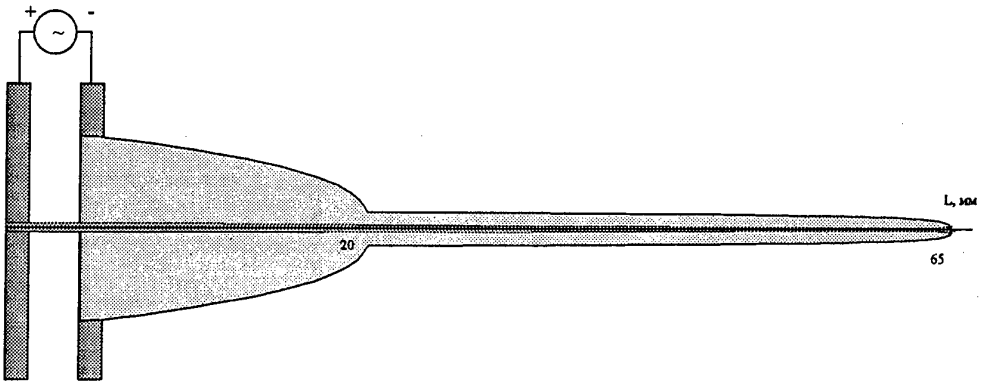

b) $T_1 \le t \le T_{BH}$, $T_1 \sim \frac{1}{2} T_{BH}$ case

Fig. 7 Radial CJ expansion: a) with current, test 10; (b) mode with $T_1 \sim \frac{1}{2} T_{BH}$

The second series of laboratory experiments was carried out using the circuit presented in Fig. 4, and cumulative charge mock-ups of diameter *30, 50, and 100 mm.*

Other EDA assemblies parameters: fiberglass insulator plates (*6*), (*7*) thickness Δ_1*=15 mm,* Δ_2*=10 mm* (for the 1st experiment), Δ_1*=20 mm,* Δ_2*=15 mm* (for the 2nd experiment), Δ_1*=30 mm,* Δ_2*=20 mm* (for the 3rd experiment). CB voltage was $V_C = 5$ *kV.*

CC shooting in all cases was normally to the target.

Experimental CJ penetration deepness *L* and energy separated in active circuit resistance W_r as a part of CB energy *W* for different CJ caliber are presented in Fig. 8.

Calculated parameters for 100-mm CJ is shown in Fig. 8.

Power losses in the active resistance *r(t)* for τ is equal to

$$W_r(W) = \int_0^{\tau_C} J^2(t) r(t) dt .$$

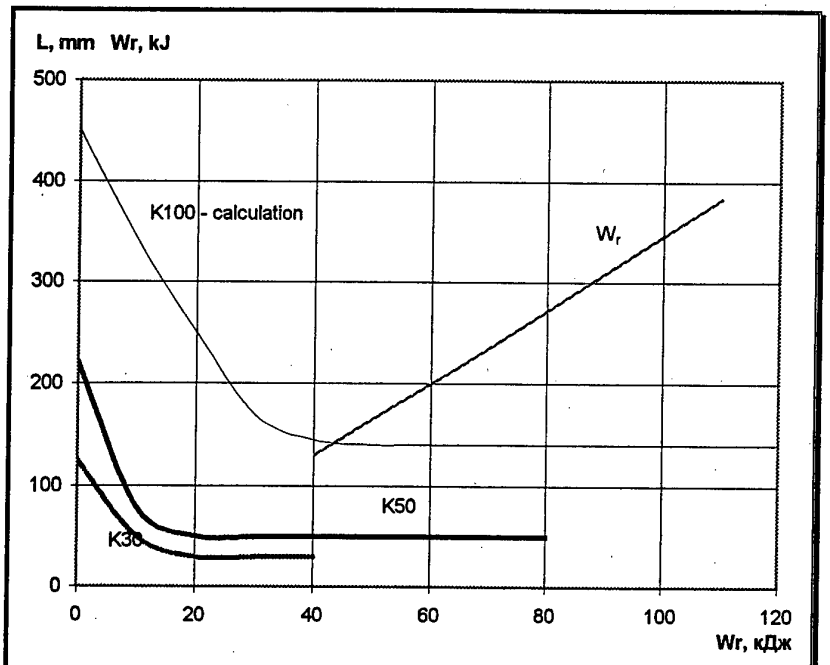

Fig. 8 Relation of CJ penetration deepness (L) and power dissipation in CJ (W_r) as functions of CB energy (W). K30, K50, K100 are charge caliber. The experimental results of IGSOAN scientific group are used

CJ current can be expressed by its density:

$$J(t) = \int_S j(t)dS = S\bar{j}(t).$$

Hence it is possible to receive the following relation for current integral:

$$\bar{\bar{I}} = \frac{W_r(W)}{\bar{r}S^2}, \qquad (15)$$

where:

$\bar{r}$ average in CJ cross-section S value of the resistance at moment of time τ.

It is interesting to compare the current integral value corresponding to explosion evaporation (blasting) of a conductor with observed in CJ experiments. For example, for 50-mm CC at $W=40\ kJ$ and $W_r(W)=1.37\ kJ$, CJ diameter $\sim 2\ mm$ and resistance $\bar{r} = 10^{-2}\ \Omega$, the current integral for a conductor blasting is estimated as $\sim 1.95\times10^{17}\ A^2 \times sec \times m^{-4}$ [3].

In the described experiments average value of the current integral was $I=1.2\times10^{16}\ A^2 \times sec \times m^{-4}$.

As it discussed in [1] blasting condition in the CJ skin-layer has not to depend on current integral. This condition can be realized at the achievement of some critical current value. For example, if $r_0 \sim 1\ mm$ $J_{cr} \sim 200\ кА$.

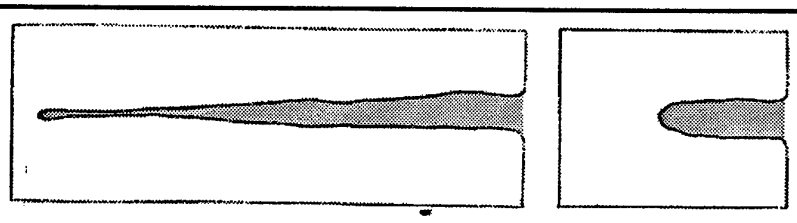

a b

Fig. 9 Cavity contours for a 50-mm CC and aluminum target. a) Test with current, b) Control test without current

It is necessary to notice that in the model of electrodynamics interaction the current integral $I = \int_0^{T_J} J(t)dt$ determines the electric charge, passing through CJ for the pulse duration T_J. Current integral for a conductor blasting $\tilde{I} = \int_0^{\tau} J^2(t)dt$ is proportional to the heating power density exuding in conductor body.

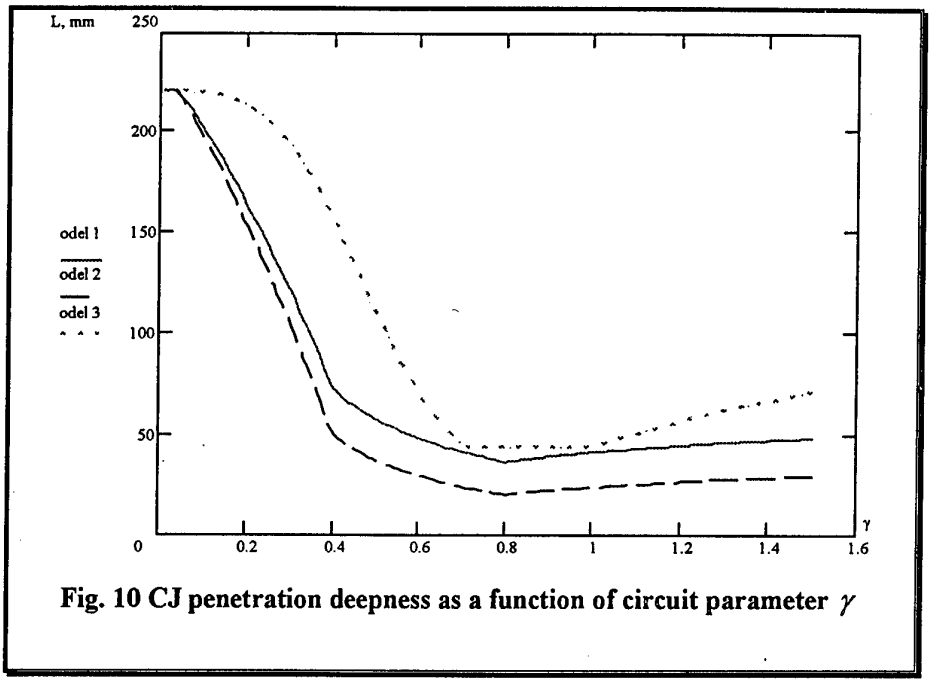

Fig. 10 CJ penetration deepness as a function of circuit parameter γ

Fig. 9 illustrates EDA efficiency in comparison of two cavity pictures drawn in the same scale for a 50-mm CC with current (a) and without current (b) in aluminum alloy *D16* target. In case a) at current *J=430 κA* L_c*=93 mm*. In case b) L_0*=360 mm.*

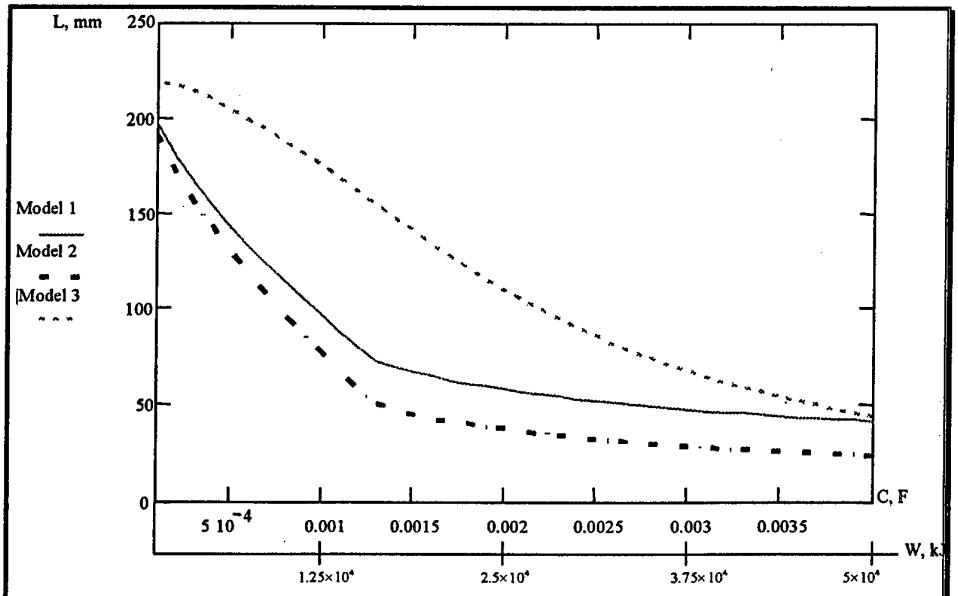

Fig. 11. Penetration deepness for 50-mm CC as a function of CB capacity and energy ($R \sim 10^{-2}\ \Omega$, $L_i = 2\times10^{-7}$ *Henry*, $V_C = 5\times10^3$ *V*)

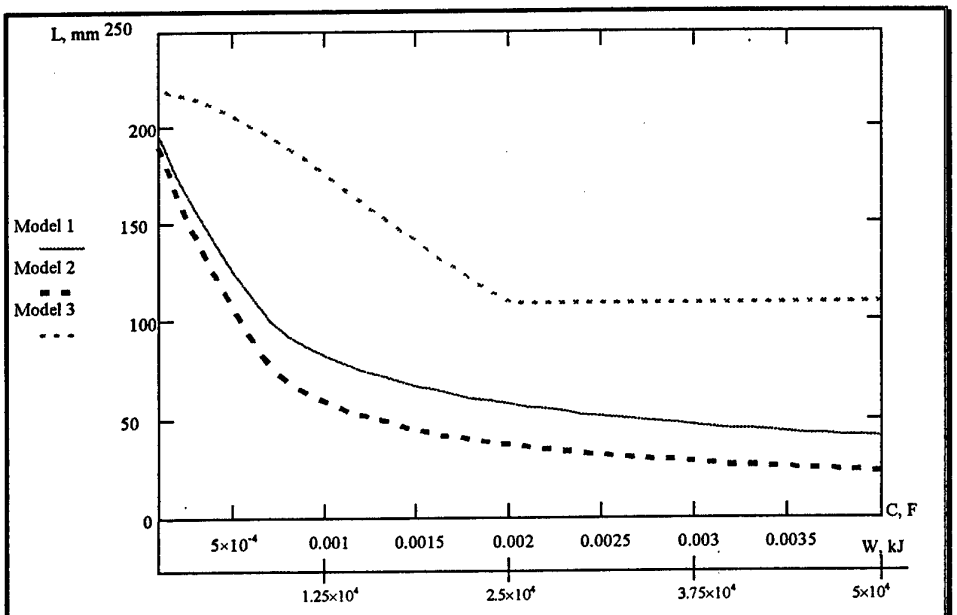

Fig.12. Penetration deepness for 50-mm CC as a function of CB capacity and energy

($R \sim 10^{-2}$ Ω, $L_i = 4 \times 10^{-7}$ Henry, $V_C = 5 \times 10^3$ V)

The average value of the CJ penetration deepness factor for caliber *K30* equals to ~*5*, for caliber *K100* equals to *2*.

Fig. 10 represents the estimation of the penetration deepness as a function of the circuit parameter $\gamma = \frac{1}{2} I \sqrt{\frac{C}{L_i}}$ calculated by different models (Appendixes 1, 3, 4) for CJ caliber $D = 50$ *mm*, circuit resistance $R = 10^{-2}$ Ω, and inductance $L_i = 2 \times 10^{-7}$ *Henry*.

At achievement of some critical value $\gamma \sim \gamma_{cr}$ the penetration deepness practically does not depend on γ.

The calculated penetration deepness as a function of the CB capacity and power (at CB voltages $V_C = 5 \times 10^3$ V) in different models (Appendixes 1, 3, 4) for CJ caliber $D = 50$ *mm* is presented in Fig. 11.

CJ penetration deepness as a function of CB capacity and energy is given in Fig. 12 at circuit inductance $L_i = 4 \times 10^{-7}$ *Henry*.

The minimum penetration deepness (Fig. 10, Fig. 11) does not depend on CB capacity (energy).

CJ penetration deepness as a functions of CB capacity and energy (at voltages $V_C = 5 \times 10^3$ V, $R \sim 10^{-2}$ Ω, $L_i = 2 \times 10^{-7}$ *Henry*) for CC of different caliber (model № 2, Appendix 3) are given in Fig.13.

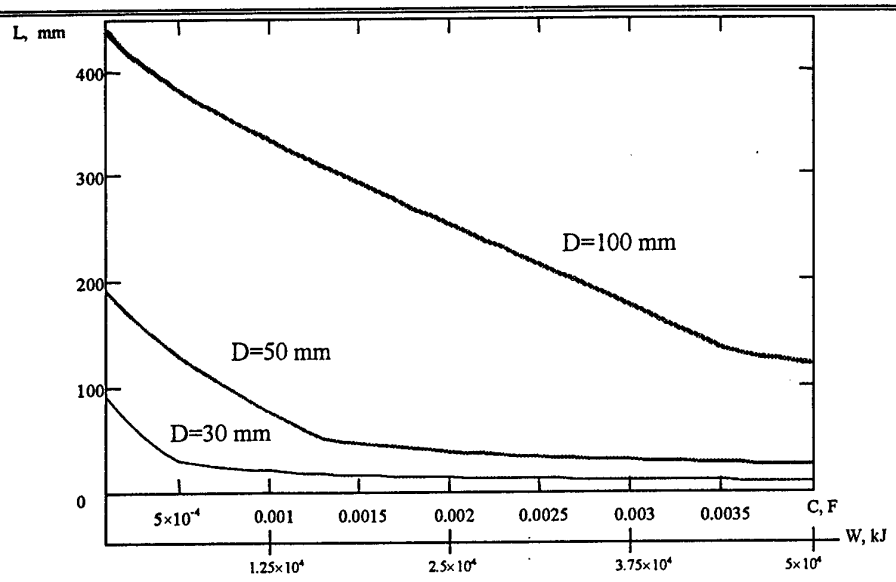

Fig. 13 Computational Estimation of the Cumulative Jet Penetration into the Bumper as a Function of the Capacity and Power of the Condenser Battery

The computational and experimental (Fig. 8) results are good correlated in the investigated range of parameters.

3 RESULTS OF EDA FULL-SCALE TESTS

The program of full-scale tests provides the demonstration of the armor efficiency of EDA with capacitor-type power supply when full-scale standard cumulative charges are used.

The tests was carried out by a scheme presented in Fig. 14. Bench units were pointed in three places. Steel container *III* and EDA mock-up *2* are placed on testing pad *II* in *50 m* away from shelter *I*. CC 1 is established near the shelter. High-voltage supply unit 4 adjusted from control panel 8 serves for CB charging to the given voltages V_C. CJ penetration initiates CB discharge. Two oscilloscopes 7 indicate the current pulse by registration signals of inductive sensors 9.

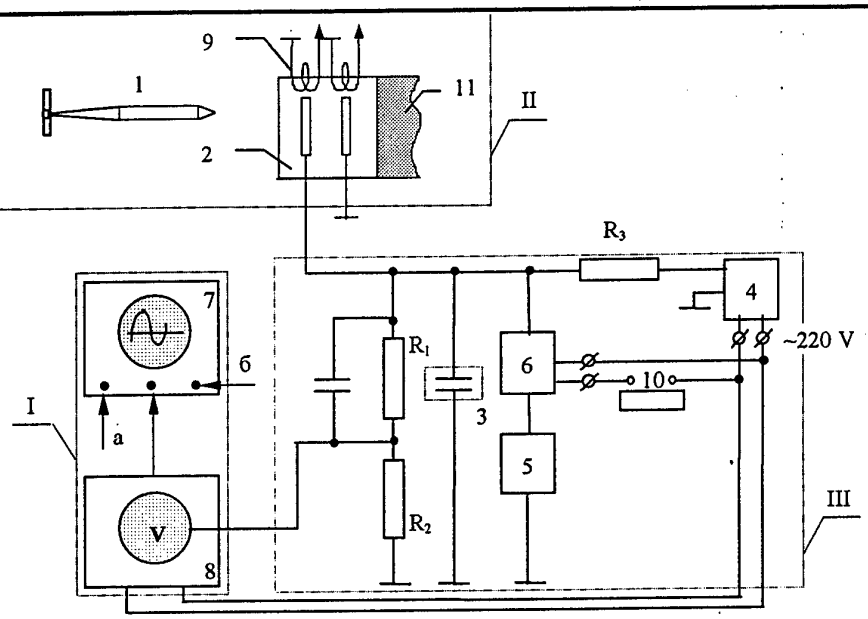

Fig. 14. EDA testing bench diagram

I – Shelter, II – Testing pad, III – Steel container, 1 – Cumulative charge, 2 – Electrical board, 3 – Capacitor battery, 4 – High-voltage supply unit, 5 – Discharge resistance, 6 – Switch, 7 – Oscilloscope, 8 – Control panel, 9 – Inductive sensors, 10 – Switch, 11 – EDA

Three-electrode EDA design diagram is given in Fig.15. Outside plate *1* is added mainly for the EDA mock-up protection against small-dimensional striking fragments. The basic plate was executed as a package of armor plates of total thickness *250 mm*.

The *90 mm* cumulative garnet was used. The range of CB parameters varying was the following:

- *1.0 kJ (C=1.0 mF, V_C=1.5 kV);*
- *5.0 kJ (C=0.4 mF, V_C=5.0 kV);*
- *12.5 kJ (C=1.0 mF, V_C=5.0 kV);*
- *17.5 kJ (C=1.4 mF, V_C=5.0 kV).*

Current maximum value in the experiments achieved *300 κA* at pulse duration 20 μs, the minimum current was *80 κA* at *12* μs.

CB storage energy varied in *1-17.5 kJ* range due to CB capacity varying.

Average penetration deepness L_0 in case of *zero* current was determined on the results of measurements in five independent experiments. It was *230 mm* at deviation within *190 mm... 250 mm.*

Experimental data are presented in Table 2 and in Fig.16.

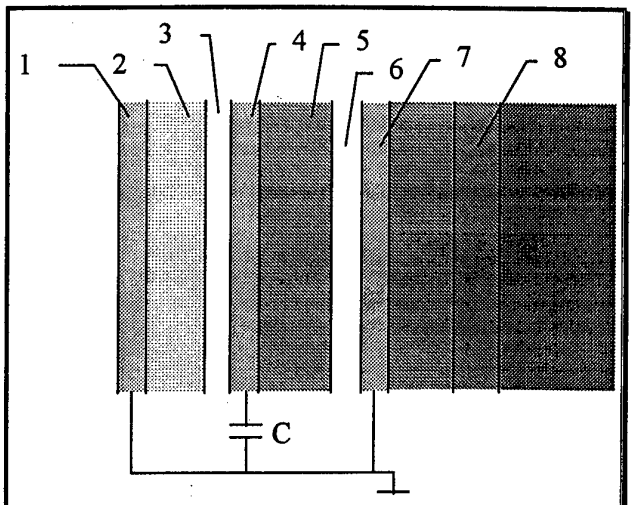

Fig.15. Three-layer EDA configuration

1 – Armor plate (16 mm*), 2 – Insulator (30 mm), 3, 6 – Air Clearance (5 mm), 4, 7 – Aluminum plates (5 mm), 5 – Insulator (25 mm), 8 – Basic armor package (target) (220 mm)

Table 2

W, *kJ*	$\bar{L}$	ΔL	$\bar{L}_0/\bar{L}$	$\bar{L}_0/L_{max}$	$\bar{L}_0/L_{min}$
1.0	178	48	1.3	1.5	15
5.0	37	59	6.2	46.0	3.6
12.5	43	76	5.3	57.0	3.9
17.5	7.5	7.0	32.0	48.0	18.4

In Fig. 16 the dependence of penetration deepness L on CB energy W is presented, as a field of experimental points not united by a curve.

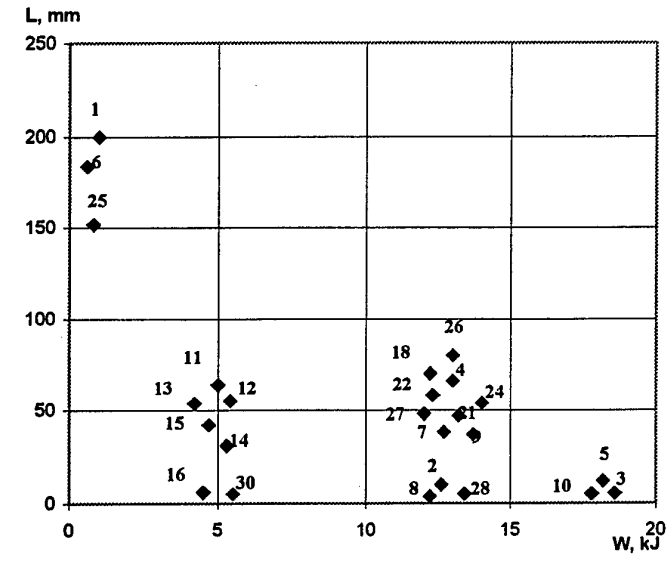

Fig. 16. Penetration deepness L as a function of CB energy *W* *for 90 mm* CC

One can see wide spread of the results. It can be explained by influence a number of factors.

- EDA electrode geometrical parameters varying;
- lower accuracy of the penetration deepness measurements;
- possible dependence of the circuit discharge resistance on weather conditions.

Never less one can see that at CB energy greater than *5 kJ* the EDA provides more than *five-time-decrease* of the penetration deepness.

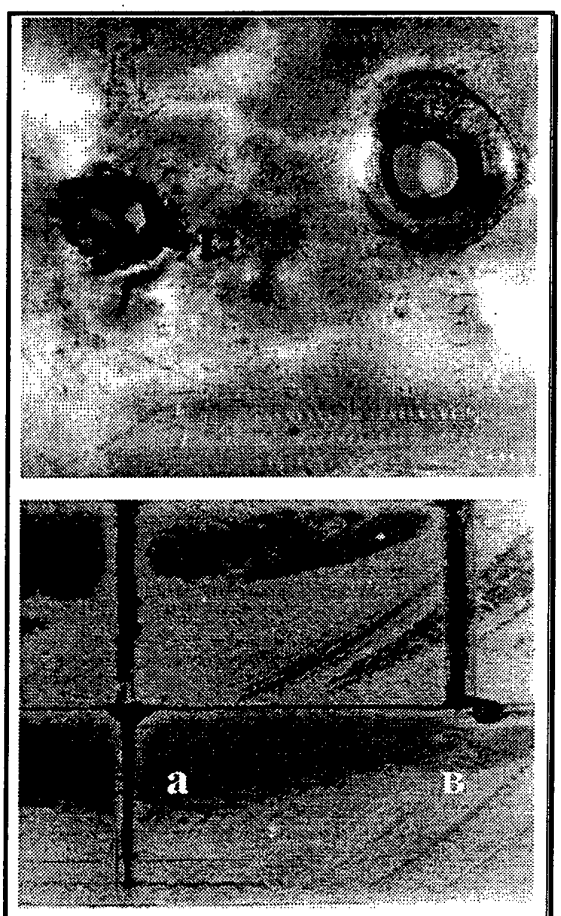

Fig.17. Photos of the Cavity Braked by Cumulative Jet in Basic Plate (a – Without Current; в – With Current) and Input Holes in the Bumper System

The photos of the cavity in basic plate (target) are shown in Fig.17. They demonstrate the influence of current on the form of cavity. The cavity in the absence of the current (left picture) is more narrow and deeper. It shows that under the current enforce the dissipation of CJ kinetic energy take place in a larger volume.

The computational dependencies of the CJ penetration deepness for the test conditions taking in calculation different circuit resistance are given in Fig. 18 at CC caliber 90 mm.

Circuit discharge resistance can be variate value mainly in the force of the equivocation of «jet - electrode» contact resistance that practically determines the total circuit discharge resistance. The results of calculations presented in Fig. 18, 19, 20 are usable for explanation of the wide spread of the experimental CJ penetration deepness data shown in Fig.16. According to Fig. 19 for example at CB energy $W=25$ *kJ* the resistance valuation in *two times* causes to calculated penetration of the detonator operation moment deepness valuation in *two times*.

Other reasons for the experimental data spread could be the dispersion of the detonator operation moment. CJ efficiency decreasing in this case maybe estimated as use of CC of smaller caliber.

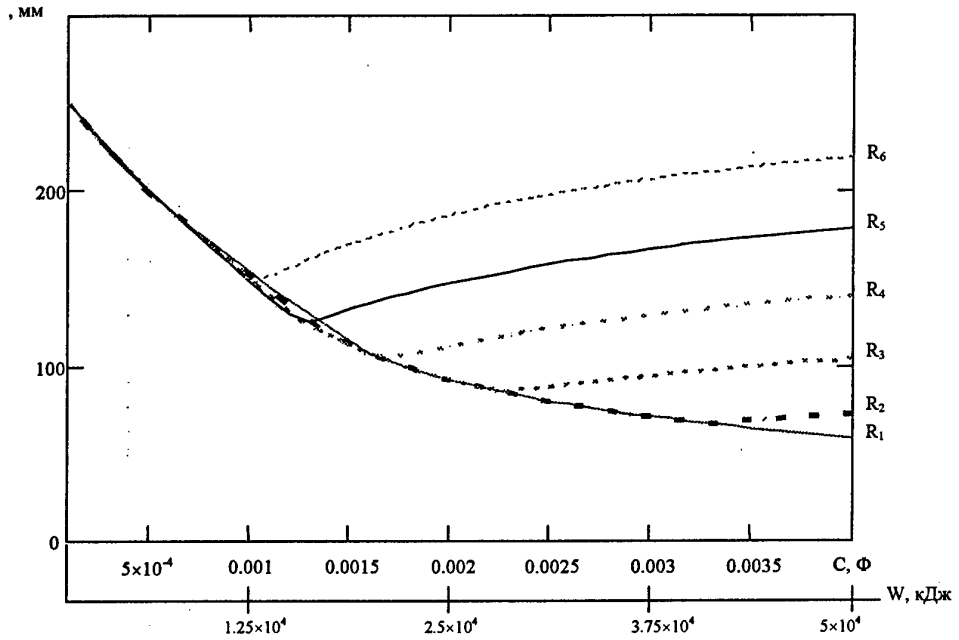

Fig. 18. Penetration deepness dependencies on CB capacity and energy and circuit resistance calculated for 90-mm CC at V_c=5×10³ V

($R_1 = 1\times10^{-2}\,\Omega$, $R_2 = 1.25\times10^{-2}\,\Omega$, $R_3 = 1.5\times10^{-2}\,\Omega$, $R_4 = 1.75\times10^{-2}\,\Omega$, $R_5 = 2\times10^{-2}\,\Omega$, $R_6 = 2.25\times10^{-2}\,\Omega$)

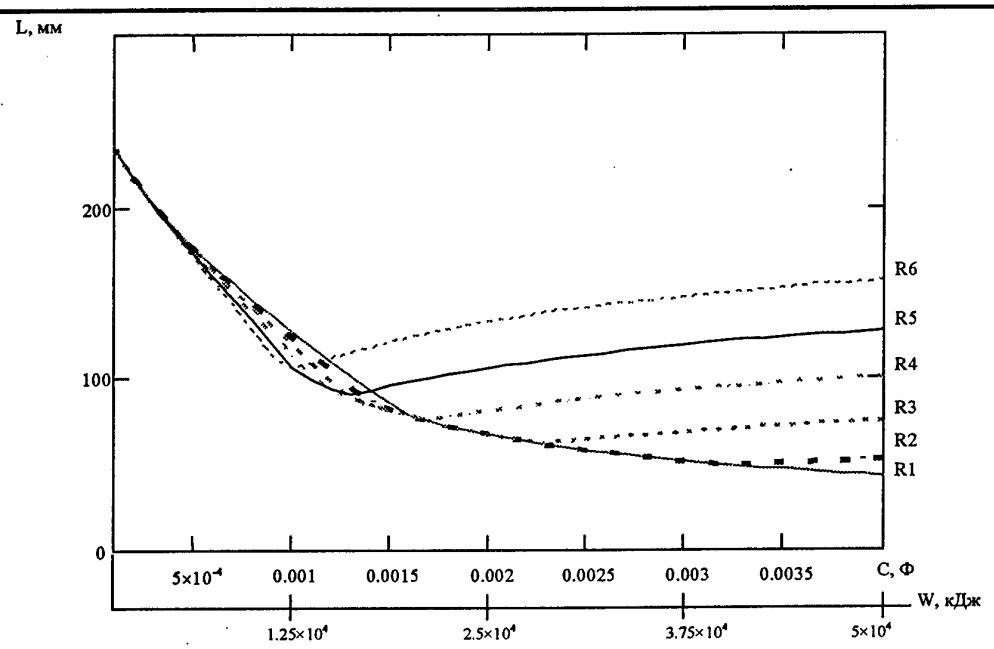

Fig. 19. Penetration deepness dependencies on CB capacity and energy and circuit resistance calculated for 70-mm CC at V_c=5×10³ V

($R_1 = 1\times10^{-2}\,\Omega$, $R_2 = 1.25\times10^{-2}\,\Omega$, $R_3 = 1.5\times10^{-2}\,\Omega$, $R_4 = 1.75\times10^{-2}\,\Omega$, $R_5 = 2\times10^{-2}\,\Omega$, $R_6 = 2.25\times10^{-2}\,\Omega$)

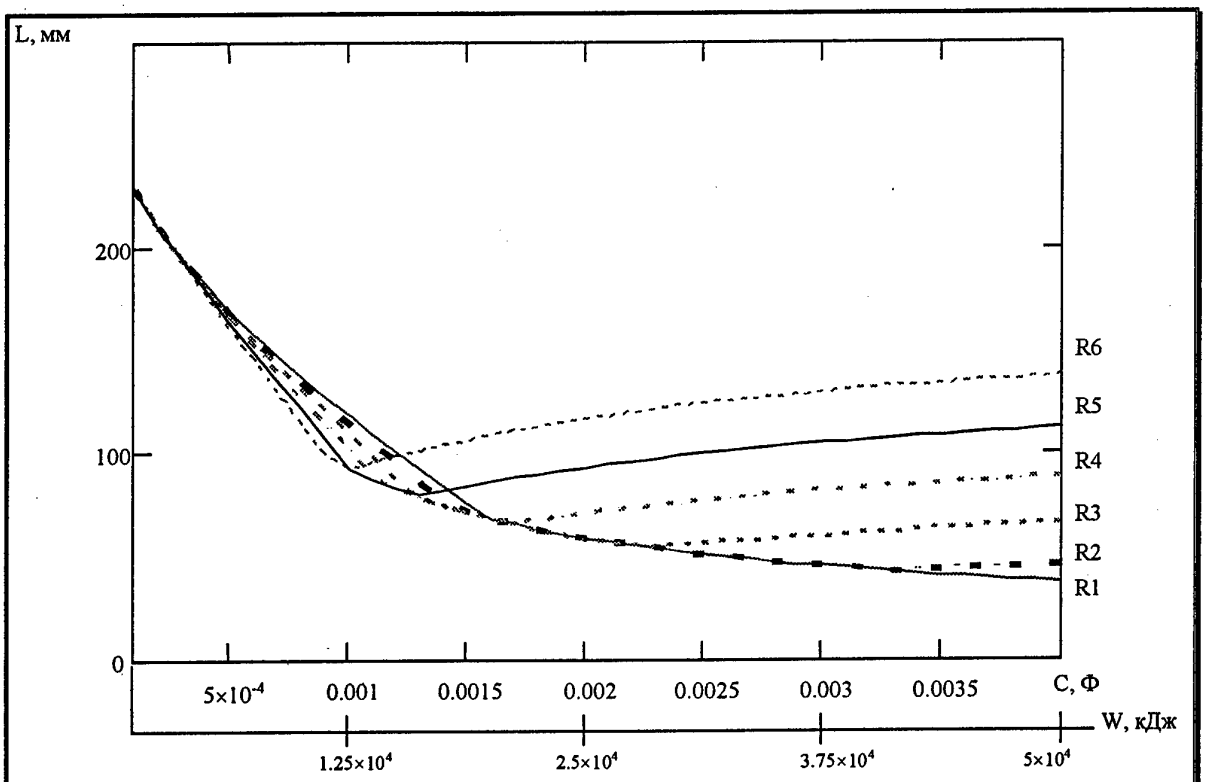

Fig. 20. Penetration deepness dependencies on CB capacity and energy and circuit resistance calculated for 90-mm CC at V_c=10×10³ V

($R_1 = 1\times10^{-2}\,\Omega$, $R_2 = 1.25\times10^{-2}\,\Omega$, $R_3 = 1.5\times10^{-2}\,\Omega$, $R_4 = 1.75\times10^{-2}\,\Omega$, $R_5 = 2\times10^{-2}\,\Omega$, $R_6 = 2.25\times10^{-2}\,\Omega$)

COCNCLUSIONS

1. EDA laboratory static tests by cumulative means of *25...100 mm* caliber shows the EDA high efficiency. Penetration deepness increasing in *five times* for *50 mm* CJ achieved. For *100 mm* caliber this value is equals to *three*.
2. Dynamics ground test result with *90 mm* standard cumulative garnet shows high instability of the results. Maximum decreasing of the CJ penetration deepness at CB power of about *25 kJ is higher than 10 times*.
3. At laboratory investigation of the EDA with the solid rod the principal possibility of its efficiency decreasing is shown, but the systematic results does not receive. Penetration deepness decreasing by *40 %* of the *7.62 mm* fairing pin was achieved.
4. EMG implementation does not allow to receive the current higher than *350 кA*, because of the generation and EDA corresponding problem did not solved.
5. The physical-and-mathematical process in EDA model usage allows to systematized the experimental investigation data on CJ with current penetration into the bumper system. The possibility of its forecasting in EDA in wide range as well as CJ parameters are established.
6. The minimum CB capacity value for the given caliber at which the EDA maximum efficiency achieved was received (CJ minimum penetration deepness). For *100 mm* CJ at CB voltage of about *~5 kV* the critical CB power value is equals to *20 kJ*.
7. The physical-and-mathematical model allowing to estimate the critical (maximum) value of the discharge circuit (interelectrode spacing resistance) at which the EDA maximum efficiency achieved in wide range of CB capacity was elaborated. For CJ caliber of about *100 mm* this resistance is equals to $\sim 10^{-2}\ \Omega$.
8. The estimation of the limited (critical) current in the cavity was carried out. It determines by the leading edge steepness of the discharge current pulse.

APPENDIX 1

ESTIMATION OF CRITICAL CURRENT AND PENETRATION DEEPNESS VALUES

A CJ motion in a magnetic field causes vortex currents in the CJ skin-layer providing the energy dissipation. When the kinetic energy losses become comparable with CJ bulk material evaporation energy, the explosive evaporation of the layer is to be. According with the proposed model a plasma cloud with metallic conductivity is implemented [1]. In case of a vortex-free plasma motion (with velocity close to CJ speed) in the magnetic field of the discharge current braking Lorentz forces begin to act. These forces are equilibrated by plasma pressure. The pressure in the plasma is transmitted through the contact surface to the CJ head resulting the penetration rate decrease.

The equation of an energy balance in the cavity [1] is the following:

$$\int_0^t \int_{r_0}^{r_l} \sigma V_p^2 B^2 U(t) 2\pi r dr dt = \frac{1}{2}\rho \pi r_0^2 \left[(V_0 - U(t))^3 - (V_0 - U_0)^3 \right] \qquad \text{A1.1}$$

Taking into account $U_0 - U(t) = \Delta U$ and expanding (A1.1) right part into a series it is possible to receive the approximate relation:

$$\int_0^t \int_{r_0}^{r_l} \sigma V_p^2 \frac{\mu^2 J^2}{2\pi r^2} r dr U(t) dt = \frac{1}{2}\rho \frac{\pi r_0^2}{2} (V_0 - U_0)^2 3\Delta U \qquad \text{A1.2}$$

The value $V_0 - U_0$ determines the jet velocity in case of penetration without the current (in coordinate system in which the contact surface is fixed).

In this case the penetration rate U_0 defines by Bernoulli's integral through pressure P in braking point onto contact surface.

$$P = \frac{1}{2}\rho U_0^2 + Y = \frac{1}{2}\rho_0 (V_0 - U_0)^2, \qquad \text{A1.3}$$

where:

Y target material strength tensile;

ρ, ρ_0 target and CJ materials densities.

Considering that

$$V_p \cong V_0 - U_0 \qquad \text{A1.4}$$

from (A1.2) one can receive (model 3):

$$\frac{L_0}{L_m} - 1 = \frac{I^2}{A_0}, \qquad \text{A1.5}$$

Where:

L_0, L_m penetration deepness without and with current respectively;

$I = J_{cr} T_{BH}$ current integral;

T_{BH} CJ penetration time;

$A_0 = \frac{6\pi M_0}{\sigma\mu^2 V_0}$

$M_0 = \rho\pi r_0^2 l_0$ CJ active part mass.

The relation (A1.5) is justice when penetration time T_{BH} is less than current pulse time T_I.

In case $T_I < T_{BH}$

$$L_m = L_0\left[\frac{1}{y+\frac{I^2}{A_0}} + 1 - \frac{1}{y}\right], \qquad \text{A1.6}$$

where:

$y = \frac{T_{BH}}{T_I} > 1.$

In [1] the model of current J excitation in the cavity by EMF deriving in the plasma layer under the influence of the magnetic field on moveable plasma flow exhausting out of the cavity has been considered.

The equation for current J calculation has the following form:

$$R_0 ZJ + L_{i0} Z\frac{\partial J}{\partial t} + L_{i0} UJ = \int_{r_I}^{r_c} V_p B(r)dr = V_p J_0 L_{i0}, \qquad \text{A1.7}$$

where:

$B = \frac{\mu J_0}{2\pi r}$;

Z penetration deepness current value;

J_0 discharge current;

V_p, U plasma velocity and penetration rate;

R_0, L_{i0} CJ linear resistance and inductance.

Approximate solution of (A1.7) in case when the discharge current determines by the front edge of a current pulse as:

$$J_0 = \frac{\partial J_0}{\partial t}t,\ Z = \overline{U}t,$$

has the fo

$$J = \frac{V_p}{\overline{U}}\frac{\partial J_0}{\partial t}\frac{L_{i0}}{R_0}\left[1 - \frac{1}{y} + \frac{exp(-y)}{y}\right],\ y = \frac{t}{t_{cr}} \qquad \text{A1.8}$$

As $\overline{U} \sim \frac{U_0}{2}$, $V_p = V_0 - U_0$, $\tilde{\gamma} \equiv \frac{V_p}{\overline{U}} \sim 2$.

$$\text{If } y >> 1,\ J \approx J_{cr} = \tilde{\gamma}\frac{\partial J_0}{\partial t}\frac{L_{i0}}{R_0} \qquad \text{A1. 9}$$

$$\text{If } y << 1,\ J \approx \frac{1}{2}\tilde{\gamma}\frac{\partial J_0}{\partial t}t$$

It is assumed for plasma conductivity calculation:

$$\sigma = \sigma_0 \frac{r_0^2}{r^2}, \qquad \text{A1.10}$$

where:

r_0 CJ radius;

r varient radius.

Note: *According to [1] the conductivity of the imperfect plasma might be presented in the following form* $\sigma = \sigma_0 \frac{n}{n_0}$, $\sigma_0 = 10^6 (\Omega \times m)^{-1}$, $n_0 \sim 10^{23} sm^{-3}$.

Plasma resistance R_0 can be calculated in approximation of a cable line including external $(r_1 < r < r_C)$ and internal $(r_0 < r < r_1)$ conductors, where r_C – cavity radius.

For this case

$$\frac{1}{R_0} = \int_{r_1}^{r_C} \sigma(r) 2\pi r dr = \sigma_0 \int_{r_1}^{r_C} \frac{r_0^2}{r^2} 2\pi r dr = \sigma_0 2\pi r_0^2 \ln\frac{r_C}{r_1}, \qquad \text{A1.11}$$

$$t_{cr} = \frac{L_{i0}}{R_0} = \mu\sigma_0 \left[\ln\frac{r_C}{r_1}\right]^2 r_0^2$$

Assuming $\ln\frac{r_C}{r_1} \sim 2$ one can receive the critical time for a CJ of $D = 100\ mm$ a value $t_{cr} \sim 10\ \mu s$.

APPENDIX 2

FORMATION OF A CURRENT CIRCUIT IN THE CAVITY

There is the mode when current J (see A1.8 at $t \geq t_{cr}$) does not achieve its critical value J_{cr} in the front of the current pulse. In this case the current in the closed circuit can be calculated according with the following assumption $J_0 = \bar{J}_0 = const$.

In this case the solution of equation A1.1 has the form:

$$J = \tilde{\gamma}\bar{J}_0 \frac{t_{cr}}{t}\left(1 - exp\left(-\frac{t}{t_{cr}}\right)\right), \quad \gamma = \frac{V_p}{\bar{U}} \sim 2 \qquad \text{A2.1}$$

$$I_1 = \int_0^{t_{cr}} J(t)dt \cong \tilde{\gamma}\bar{J}_0 t_{cr}$$

$$I_2 = \int_{t_{cr}}^{T_1} J(t)dt \cong \tilde{\gamma}\bar{J}_0 t_{cr}\, ln\frac{T_1}{t_{cr}}$$

The current integral is

$$I = I_1 + I_2 = \tilde{\gamma}\bar{J}_0 t_{cr}\left(1 + ln\frac{T_1}{t_{cr}}\right). \qquad \text{A2.1}$$

Thus, the problem of the determination of the current integral reduces to the problem of the calculation of the average discharge current $\bar{J}_0$.

Analysis of the experimental data shows that the modes with CB minimum energy when the penetration decrease is visible are close to the critical discharge mode ($\gamma \sim 1$).

In this case $T_1 \sim T_{BH}$. If $\gamma = 1$ the current is determined as:

$$J_0 = \frac{V_c}{L_i} t\, exp(-\delta t), \qquad \text{A2.3}$$

where:

$\delta = \dfrac{R}{2L_i}$ dumping decrement.

Let us determine the critical value of the discharge current:

$$\bar{J}_0^{cr} = \frac{V_C}{L_i}\frac{1}{T_{BH}}\int_0^{T_{BH}} t\, exp(-\delta t)dt \cong \frac{V_C C_{cr}}{T_{BH}}, \quad \gamma = 1. \qquad \text{A2.2}$$

For example, if $V_0 \sim 5 \times 10^3$ V, $L_i \sim 2 \times 10^{-7}$ Henry, $R = 10^{-2}\ \Omega$, $T_1 = T_{BH} \sim 100\ \mu s$, current pulse duration $T_1(\gamma = 1) \to \infty$ (see Fig. 3), one can receive $\bar{J}_0 = 400\ \kappa A$.

To estimate $\bar{J}_0$ we need to define the corrected relation at γ as variate (for example, at CB capacity valuation).

It gives [3]:

1. in case $\gamma < 1$:

$$J = \frac{V_C}{\omega L_i} exp(-\delta t) Sin\omega t\ ,\ \omega = \omega_0 \sqrt{1-\gamma^2}\ ,\ \omega_0 = \frac{1}{\sqrt{L_i C}}\ ,\ \delta = \frac{R}{2L_i}\ ,\ \gamma = \frac{1}{2} R \sqrt{\frac{C}{L_i}} \qquad \text{A2.3}$$

2. in case $\gamma > 1$:

$$J = \frac{V_C}{\omega^* L_i} exp(-\delta t) \frac{e^{\omega^* t} - e^{-\omega^* t}}{2}\ ,\ \omega^* = \omega_0 \sqrt{\gamma^2 - 1}\ . \qquad \text{A2.4}$$

Expanding in series $Sin\omega t$ and ($e^{\omega^* t}$ and $e^{-\omega^* t}$) one can receive the approximate relation for current:

1. in case $\gamma < 1$:

$$J = \frac{V_C}{L_i} t\, exp(-\delta t) \left[1 - \frac{(\omega t)^2}{6} \right] \qquad \text{A2.5}$$

2. in case $\gamma > 1$:

$$J = \frac{V_C}{L_i} t\, exp(-\delta t) \left[1 + \frac{(\omega^* t)^2}{6} \right]. \qquad \text{A2.6}$$

Averaging the relations for a current pulse we receive:

$$\bar{J}_0 = \bar{J}_0^{cr} \frac{1+\gamma^2}{2\gamma^2}\ . \qquad \text{A2.7}$$

$$\text{For } T_i < T_{BH}\ \ \bar{J}_0 = \bar{J}_0^{cr} \frac{1+\gamma^2}{2\gamma^2} \frac{T_{BH}}{T_i}$$

At $\gamma = 1$ $\bar{J}_0 = \bar{J}_0^{cr}$.

Relation (A.2.7) can be transformed to:

$$\bar{J}_0 = \frac{V_C C}{T_I} \frac{1}{2} \frac{1+\gamma^2}{\gamma^2}\ . \qquad \text{A2.8}$$

For $\gamma << 1$ the current is calculated by the following formula:

$$\bar{J}_0 = \frac{q_0}{T_I / 2} = \frac{2 V_C C}{T_I}\ , \qquad \text{A2.9}$$

where:

q_0 CB capacity.

Relation (A2.8) transmitted to relation (A2.9) at $\gamma \sim 0.8$.

APPENDIX 3

MODEL OF THE ELECTRODYNAMIC BRAKING UNDER CJ RADIAL DEFORMATION

The model assumes that the discharge current mainly flows through CJ and closed in the cavity on the contact surface separated CJ and the target. The effect of CJ penetration deepness decrease is connected with the braking of CJ head part because of magnetic pressure and viscosity forces' work.

The work carried out against the force of the magnetic pressure causes Lorentz force operation with density:

$$F_L = j_Z B_\varphi = \sigma\left(E_Z + V_r B_\varphi\right) B_\varphi ,$$

where:

V_r radial component of CJ velocity near the contact surface;

E_Z axial electric field strength;

σ CJ material conductivity;

$B_\varphi = \dfrac{\mu J^2}{2\pi r}$.

As current j_Z induces and closes in skin-layer limits the total current is equals zero and $E_z \sim 0$ (accurately E_Z determines by the main current flow conditions and this value can be neglect).

Stationary Navier-Stokes equation for CJ radial velocity V_r on arbitrary radius r in cylindrical coordinates can be assumed as follows:

$$(V\nabla)V_r = -\frac{1}{\rho_C}\frac{\partial P}{\partial r} + \nu \Delta V_r ,$$

where:

$$(V\nabla) \equiv V_r \frac{\partial V_r}{\partial r} + V_Z \frac{\partial V_r}{\partial z},\quad \Delta V_r \equiv \frac{1}{r}\frac{\partial}{\partial r}\left(r\frac{\partial V_r}{\partial r}\right) + \frac{\partial^2 V_r}{\partial z^2} \qquad \text{A3.1}$$

Continuity equation:

$$\frac{1}{r}\frac{\partial}{\partial r}\left(rV_r\right) + \frac{\partial V_Z}{\partial z} = 0 ,$$

A3.2

Conservation equation of an axial flow:

$$\tilde{R}^2 V_Z = r_0^2 V_0 ,$$

A3.3

where:

P pressure in CJ;

ρ_C, ν CJ material density and viscosity;

$\tilde{R}, r, r_0$ external, current and initial CJ radiuses;

V_z axial jet velocity.

Axial coordinate $z = 0$ corresponds to CJ cross-section near the internal electrode, $z = l$ is a position near the contact surface.

In assumption that $\frac{\partial V_r}{\partial z} >> \frac{\partial V_r}{\partial r}$ Navier-Stokes equation transforms to:

$$V_z \frac{\partial V_r}{\partial z} = -\frac{1}{\rho}\frac{\partial P}{\partial r} + \nu \frac{\partial^2 V_r}{\partial z^2},$$

A3.4

Equations A3.1...A3.4 can be solved taking into account the following assumption

$$V_r = V_r(r,z),\ V_z = V_z(z),\ P(z) = const..$$

Boundary conditions:

$$V_r|_{Z=0} = 0\ ,\ V_r|_{Z=l} = 0$$

$$V_Z|_{Z=0} = V_0$$

$$P\left(r = \tilde{R}\right) = P_M = \frac{\mu J^2}{8\pi^2 \tilde{R}^2},$$

where:

$\tilde{R}$ internal CJ radius;

l CJ part of length between the internal electrode and the contact surface.

Taking the integral of equation (A3.4) it is possible to receive the following estimation:

$$V_r = -\frac{\partial V_Z}{\partial z}\frac{r}{2} + \frac{B_1}{r}.$$

Boundary condition $V_r|_{r=0} = 0$ brings the relation:

$$V_r = -\frac{\partial V_Z}{\partial z}\frac{r}{2}.$$

A3.5

In equation (A3.5) $V_Z(z)$ value is replaced by its average mean $\overline{V}_Z$:

$$\overline{V}_z \frac{\partial V_r}{\partial z} = -\frac{1}{\rho}\frac{\partial P}{\partial r} + \nu \frac{\partial^2 V_r}{\partial z^2}$$

A3.6

Boundary conditions:

- $z = 0, V_r \cong 0 \left(\frac{\partial V_r}{\partial r} = 0\right)$;
- $z = l, V_r = 0$ for viscous liquid on solid surface.

The solution of (A3.6) is the following:

$$V_r = \frac{1}{\eta}\frac{\partial P}{\partial r}\frac{l - z}{\alpha},\ \alpha = \frac{\overline{V}_z}{\nu},\ \eta = \rho\nu$$

A3.7

From equations (A3.6) and (A3.7) follows:

$$\frac{\partial P}{\partial r} = -\eta \frac{\partial V_z}{\partial z} \frac{r}{2} \frac{\alpha}{l - z} \qquad \text{A3.8}$$

Equation (A3.8) has the solution:

$$P(r) = -\eta \frac{\partial V_z}{\partial z} \frac{\left(\widetilde{R}^2 - r^2\right)}{4} \frac{\alpha}{l - z} + P_M ,$$

where:

P_M magnetic pressure on CJ boundary $r = \widetilde{R}$.

Averaging $P(r)$ over the radius and taking into account that $P = P_0 = \frac{\mu J^2}{8\pi^2 r_0^2}$ ($P(z) = const$), it is possible to receive:

$$a_0(1 - y) = -\frac{1}{6}\eta \frac{\alpha}{l - z} \frac{dy}{dz} \frac{1}{y} \left(a_0 = \frac{\mu J^2}{8\pi^2 r_0^4 V_0};\ y = \frac{V_z}{V_0};\ \alpha = \frac{\overline{V}_z}{\nu}\right) \qquad \text{A3.9}$$

The integral of (A3.9) with boundary condition $y(0) = 1$ is:

$$y(z) = \frac{V_z}{V_0} = exp\left(-m\xi^2\right),\ m = 1.5\left(\frac{l}{r_0}\right)^2 \frac{P_M}{P_G} \frac{1}{\overline{y}},\ \xi = \frac{z}{l} \qquad \text{A3.10}$$

Whence:

$$\overline{y} = \frac{\overline{V}_z}{V_0} = \int_0^1 y(\xi) d\xi = \int_0^1 exp\left(-m\xi^2\right) d\xi = \int_0^{\sqrt{m}} \frac{exp\left(-\beta^2\right)}{\sqrt{m}} d\beta = \frac{\sqrt{\pi}}{2} \frac{1}{\sqrt{m}} erf\sqrt{m} \qquad \text{A3.11}$$

For $\sqrt{m} >> 1$ we have $efr\sqrt{m} \sim 1$. Then:

$$\overline{y} \cong \frac{1}{2}\left(\frac{r_0}{l}\right)^2 \frac{P_G}{P_M} \qquad \text{A3.12}$$

Or

$$\frac{1}{\overline{y}} = \frac{V_0}{\overline{V}_z} = \frac{U_0}{\overline{U}} = \frac{L_0}{L_m} = 2\left[\frac{l}{r_0}\right]^2 \frac{P_M}{P_G}, \qquad \text{A3.13}$$

where:

$l = d + L_m$

d interelectrode spacing;

L_0, L_m penetration deepness without and with current.

For $l = l_{min} = d$ we have:

$$\left(\frac{L_0}{L_m}\right) > 1 \text{ at } \frac{d}{r_0} > \sqrt{\frac{1}{2}\frac{P_G}{P_M}}. \qquad \text{A3.14}$$

At $J = 400\ \kappa A$, $r_0 \sim 1\ mm$, $\frac{P_G}{P_M} = 125$, $d > 10\ mm$.

In case $L_m >> d$, $l \sim L_m$ and equation (A3.13) has a view:

$$\frac{L_0}{L_m} = 1.25\left(\frac{L_0}{r_0}\right)^{\frac{2}{3}}\left(\frac{P_M}{P_G}\right)^{\frac{1}{3}} \text{ (model № 2),} \qquad \text{A3.15}$$

For CJ with $r_0 \sim 1.5\ mm$, $L_0 = 250\ mm$ at current $J \sim 400\ \kappa A$ factor $\frac{L_0}{L_m} \sim 5$. At current $J \sim 200\ \kappa A$ the factor $\frac{L_0}{L_m} \sim 3$.

In the result of the estimations it is possible to note the following:

- The model of CJ electrodynamics braking is developed taking into the viscosity. However the penetration deepness does not depend on viscosity.
- The penetration deepness decrease factor is determined by *two parameters* – relation between penetration deepness without the current and initial CJ radius and by the ratio of the magnetic pressure to the hydrodynamics pressure.
- Calculated penetration deepness decrease factor *is close* to experimentally observed values.

APPENDIX 4

«PLANE» MODEL OF JET ELECTRODYNAMICS BRAKING INFLUENCING BY JET TRANSVERS DEFORMATION

The hydrodynamics model for which the assumption of pressure constancy along CJ is not needed (as it is assumed in model № 2) is discussed.

The mathematical model is based on the analytical solution when the viscosity term in Navier-Stokes equation is neglected.

Note: the possibility of this approach was looked in Appendix 3, where it was shown that penetration deepness does not depend on CJ viscosity.

The problem can pose as follows.

It is necessary to determine CJ velocity valuation and hydrodynamics pressure valuation at axial symmetrical moving at the conditions:

- At $r = 0$ CJ is asymptotically represented by a cylinder of r_0 radius the axis of which agrees with Z and its axial velocity is V_0.
- At $r = l$,infinity target is pointed. The contact surface velocity is U.
- In CJ plane impact there is formed a wave of radial deformation.
- Current J_0 flows on CJ free jet surface. This current generates the magnetic pressure $P_M = \frac{\mu J^2}{8\pi^2 \tilde{R}^2}$, where $\tilde{R}$ – distance from CJ axis.

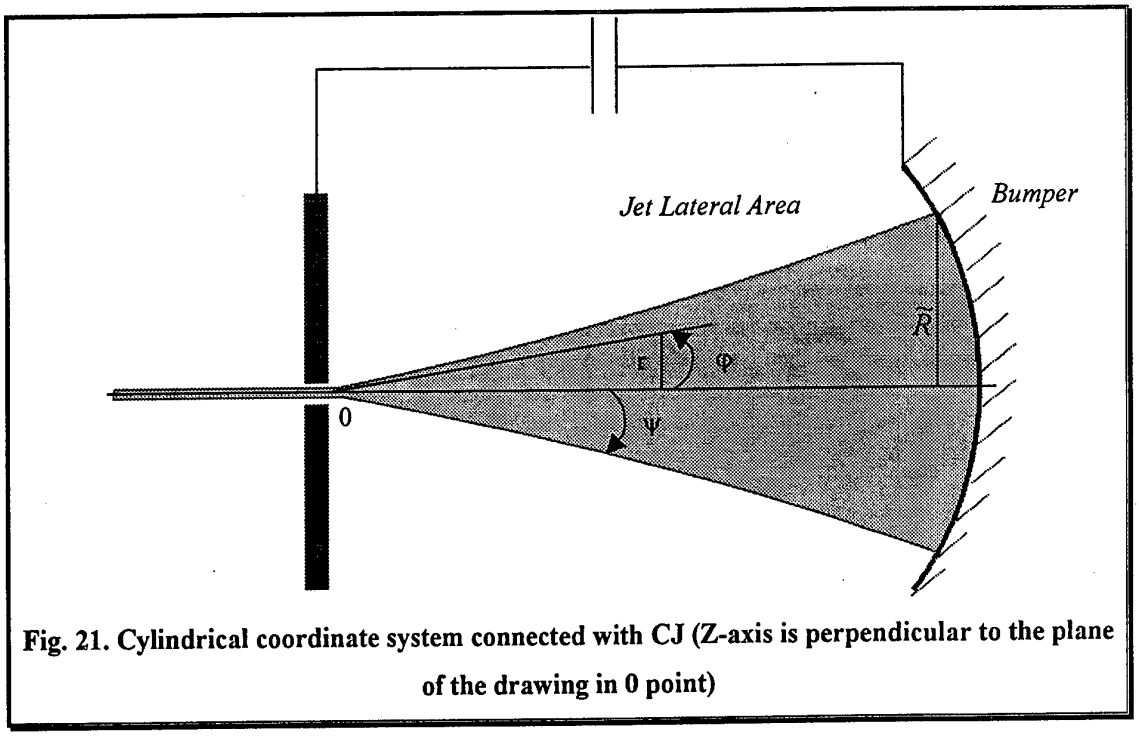

Fig. 21. Cylindrical coordinate system connected with CJ (Z-axis is perpendicular to the plane of the drawing in 0 point)

The plane option of the problem is considered in spite of the cylindrical coordinates are selected (see Fig. 21). The motion is considered in plane with the coordinates r, z, φ. Axis Z is perpendicular to the drawing plane. The motion along Z axis is absent, but $V_r = V_r(r)$, $V_\varphi = V_l(r, \varphi)$.

Two-component-steady-state Navier-Stokes equation are taken into account [5]:

$$(V\nabla)V_r - \frac{V_\varphi^2}{r} = -\frac{1}{\rho}\frac{\partial P}{\partial r},$$

$$(V\nabla)V_\varphi + \frac{V_r V_\varphi}{r} = -\frac{1}{\rho^2}\frac{\partial P}{\partial \varphi} \qquad \text{A4.1}$$

For $V_\varphi << V_r$ it is possible to receive:

$$V_r\frac{\partial V_r}{\partial r} = -\frac{1}{\rho}\frac{\partial P}{\partial r},$$

$$V_r\left(\frac{\partial V_\varphi}{\partial r} + \frac{V_\varphi}{r}\right) = -\frac{1}{\rho r}\frac{\partial P}{\partial \varphi} \qquad \text{A4.2}$$

Continuity equation:

$$\frac{1}{r}\frac{\partial(rV_r)}{\partial r} + \frac{1}{r}\frac{\partial V_\varphi}{\partial \varphi} = 0$$

has the following solution ($V_\varphi << V_r$)

$$rV_r = M(\varphi), \qquad \text{A4.3}$$

In case when CJ is moving as a whole

$$M(\varphi) = M(\psi), \text{ where } \psi = \varphi_{max}. \qquad \text{A4.4}$$

Equations(A4.1..A4.2), give the result:

$$M(\psi)\frac{1}{r}\frac{\partial}{\partial r}(rV_\varphi) = -\frac{1}{\rho}\frac{\partial P}{\partial \varphi} \qquad \text{A4.5}$$

From the equations(A4.3..A4.4) neglecting the pressure one can receive:

$$M(\psi)\frac{\partial}{\partial r}\left(\frac{1}{r}\frac{\partial}{\partial r}(rV_\varphi)\right) - \frac{\partial}{\partial \varphi}\frac{\partial}{\partial r}\left(\frac{V_r^2}{2}\right) = 0. \qquad \text{A4.6}$$

The integration gives the following relation:

$$M(\psi)\left[\frac{1}{r}\frac{\partial}{\partial r}(rV_\varphi)\right] - \frac{\partial}{\partial \varphi}\left(\frac{V_r^2}{2}\right) = f(\varphi). \qquad \text{A4.7}$$

Having $V_r = V_r(r)$, one can find:

$$M(\psi)\left[\frac{1}{r}\frac{\partial}{\partial r}(rV_\varphi)\right] = f(\psi).$$

A4.8

Equations (A4.6) and (A4.7) are identical in the case:

$$f(\psi) = -\frac{1}{\rho}\frac{\partial P}{\partial \varphi}.$$

A4.9

Integral of (A4.9) is:

$$f(\psi)\psi = -\int_0^{\psi}\frac{1}{\rho}\frac{\partial P}{\partial \varphi}d\varphi = -\frac{1}{\rho}[P(\psi) - P(0)] = -\frac{1}{\rho}[(P_0 - P_M) - P_o] = \frac{1}{\rho}P_M,$$

A4.10

where:

P_0 hydrodynamics pressure.

Integral of (A4.10) if to take into account (A4.9) is:

$$V_\varphi = \frac{1}{2}\frac{f(\psi)r}{M(\psi)} \equiv \frac{1}{2\rho}\frac{P_M r}{M(\psi)\psi},$$

A4.11

The radial velocity valuation V_r is determined from equation:

$$\frac{dR}{dt} = \frac{dR}{dr}V_r \approx V_\varphi$$

Or

$$V_r\left(\psi + r\frac{\partial \psi}{\partial r}\right) = V_\varphi$$

A4.12

From (A4.11) and (A4.12) taking into account the flow conservation equation in a form :

$$V_r\tilde{R} = V_0 r_0,$$

A4.13

it is possible to receive

$$1 + r^*\frac{1}{\psi}\frac{\partial \psi}{\partial r^*} = \frac{1}{2}\frac{P_M}{P_G}\frac{l^2}{r_0^2}r^*, \quad r^* = \frac{r}{l}$$

A4.14

The solution of (A4.14) at condition $V_r = \frac{V_0 r_0}{\tilde{R}} = \frac{V_0 r_0}{\psi r}$ and $V_r(r_0) \equiv V_0$ is:

$$\frac{V_r}{V_0} = exp\left(-\frac{1}{2}\frac{P_M}{P_G}\frac{l^2}{r_0^2}r^{*2}\right).$$

A4.15

Averaging V_r on r^* in interval $[0,1]$, it is possible to receive:

$$\bar{y} = \frac{\bar{V}_r}{V_0} = \int_0^1 y(r^*)dr^* = \int_0^{\sqrt{m}} \frac{exp(-\beta^2)}{\sqrt{m}} d\beta = \frac{\sqrt{\pi}}{2}\frac{1}{\sqrt{m}} erf\sqrt{m} \approx \frac{\sqrt{\pi}}{2}\frac{1}{\sqrt{m}};$$

$$\left(m > 1, erf\sqrt{m} \approx 1\right),\ \sqrt{m} = \sqrt{\frac{1}{2}}\sqrt{\frac{P_M}{P_G}\frac{l}{r_0}} \cong 0.7\sqrt{\frac{P_M}{P_G}\frac{l}{r_0}} \qquad \text{A4.16}$$

Whence

$$\frac{V_0}{\bar{V}_r} = \sqrt{\frac{1}{2}}\sqrt{\frac{P_M}{P_G}\frac{l}{r_0}}. \qquad \text{A4.17}$$

For $l = l_{min} = d$ $(l = d + L_m)$, where L_m – penetration deepness, the condition $\frac{L_0}{L_m} > 1$ is realized at $\frac{d}{r_0} > \sqrt{\frac{\pi}{2}}\sqrt{\frac{P_G}{P_M}}$.

For $(J = 400\ \kappa A,\ r_0 \sim 1\,mm,\ \frac{P_G}{P_M} \approx 125,\ d \geq 15\,mm)$.

At last from (A4.17) we can find: $\frac{V_0}{\bar{V}_r} = \frac{U_0}{\bar{U}} = \frac{L_0}{L_m} = \sqrt{\frac{2}{\pi}}\sqrt{\frac{P_M}{P_G}\frac{L_m}{r_0}}$

or

$$\frac{L_0}{L_m} \cong \left[\frac{P_M}{P_G}\right]^{\frac{1}{4}}\left[\frac{L_0}{r_0}\right]^{\frac{1}{2}} \text{ (model 1)} \qquad \text{A4.18}$$

For $r_0 \sim 1\,mm$, $L_0 \approx 250\ mm$, discharge current $J = 400\ \kappa A$, decrease factor $\frac{L_0}{L_m} \cong 3.3$. Taking for the discharge current a value $J = 200\ \kappa A$ we find decrease deepness factor to be equal to $\frac{L_0}{L_m} \cong 2.3$.

For the case when the penetration finishes in the front of the current pulse we can receive:

$$J(t) = J_{max}\frac{t}{t_{max}} \sim J_{max}\frac{t}{T_{BH}}.$$

The approximate expression for penetration deepness is followed from (A4.18):

$$\frac{V_0}{\bar{V}_x} = \frac{1}{T_{BH}}\int_0^{T_{BH}} \sqrt{\frac{2}{\pi}}\sqrt{\frac{P_M^{max}}{P_G}}\frac{t}{T_{BH}}\bar{V}_x dt,\ \left(P_M^{max} = P_M(J_{max})\right),\ \frac{V_0}{\bar{V}_x} = \frac{1}{3}\sqrt{\frac{2}{\pi}}\sqrt{\frac{P_M^{max}}{P_G}}\frac{L_m}{r_0},$$

$$\frac{L_0}{L_m} \sim 0.6\left[\frac{P_M^{max}}{P_G}\right]^{\frac{1}{4}}\left[\frac{L_0}{r_0}\right]^{\frac{1}{2}}. \qquad \text{A4.19}$$

REFERENCES

1. Report on Subject. Stage 1. 1998.
2. Report on Subject. Stage 2. 1999 r.
3. H. Knoepfel. Pulsed High Magnetic Fields. 1970.
4. A.Ya. Sagomonyan. Dymanics of the Bumper Penetration. Moscow.: MSU, 1988, pp. 40 – 43 (Rus.).
5. L.D. Landau. Hydrodynamics. M.: Nauka, 1988 (Rus.).
6. G.A. Shvetshov, A.D. Morozov. Experimental Investigation of the Cumulative Jet Current Instabilities. In the Proceeding of the 7th International Conference on Megagauss Magnetic Field Generation and Related Experiments, Sarov, 5...10 August 1996. "Megagauss and Megaamper Pulse Technology and Applications". V. 2. Sarov, VNIIEPh. 1996, pp. 979 – 986.
7. J.A. Shercliff. A Textbook of Magnetohydrodynamics. New York. 1965.